





Review

Recent Advances in Protective Coatings for Accident Tolerant Zr-Based Fuel Claddings

Egor Kashkarov ^{1,*} , Bright Afornu ¹ , Dmitrii Sidelev ¹ , Maksim Krinitcyn ^{2,3} , Veronica Gouws ¹ and Andrey Lider ¹

¹ School of Nuclear Science and Engineering, National Research Tomsk Polytechnic University, Lenin Avenue 30, 634050 Tomsk, Russia; brightafornu@yahoo.com (B.A.); sidelevdv@tpu.ru (D.S.); kgabeyvero@gmail.com (V.G.); lider@tpu.ru (A.L.)

² School of Advanced Manufacturing Technologies, National Research Tomsk Polytechnic University, Lenin Avenue 30, 634050 Tomsk, Russia; krinmax@gmail.com

³ Institute of Strength Physics and Materials Science SB RAS, Akademicheskii Avenue 2/4, 634055 Tomsk, Russia

* Correspondence: ebk@tpu.ru; Tel.: +7-(3822)-701777 (ext. 1562)

Abstract: Zirconium-based alloys have served the nuclear industry for several decades due to their acceptable properties for nuclear cores of light water reactors (LWRs). However, severe accidents in LWRs have directed research and development of accident tolerant fuel (ATF) concepts that aim to improve nuclear fuel safety during normal operation, operational transients and possible accident scenarios. This review introduces the latest results in the development of protective coatings for ATF claddings based on Zr alloys, involving their behavior under normal and accident conditions in LWRs. Great attention has been paid to the protection and oxidation mechanisms of coated claddings, as well as to the mutual interdiffusion between coatings and zirconium alloys. An overview of recent developments in barrier coatings is introduced, and possible barrier layers and structure designs for suppressing mutual diffusion are proposed.

Keywords: protective coatings; high temperature oxidation; corrosion; fuel claddings; zirconium-based alloys; accident tolerant fuel; interdiffusion; barrier layers



Citation: Kashkarov, E.; Afornu, B.; Sidelev, D.; Krinitcyn, M.; Gouws, V.; Lider, A. Recent Advances in Protective Coatings for Accident Tolerant Zr-Based Fuel Claddings. *Coatings* **2021**, *11*, 557. <https://doi.org/10.3390/coatings11050557>

Academic Editor: Robert B. Heimann

Received: 2 April 2021

Accepted: 7 May 2021

Published: 9 May 2021

Publisher's Note: MDPI stays neutral with regard to jurisdictional claims in published maps and institutional affiliations.



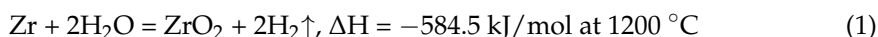
Copyright: © 2021 by the authors. Licensee MDPI, Basel, Switzerland. This article is an open access article distributed under the terms and conditions of the Creative Commons Attribution (CC BY) license (<https://creativecommons.org/licenses/by/4.0/>).

1. Introduction

In recent decades, zirconium-based alloys have been used in the nuclear industry as the main material for fuel claddings and other structural components of pressurized and boiling water reactors (PWRs and BWRs), Russian water–water energetic reactors (VVERs) and high-power channel-type reactors (RBMK) [1]. During normal operation, zirconium alloys form a protective zirconium oxide layer that reduces cladding corrosion in the coolant. The key factors affecting claddings degradation are radiation swelling and embrittlement caused by oxidation and hydrogenation of the zirconium claddings [2–4]. However, zirconium alloys demonstrate poor oxidation kinetics at elevated temperatures. Since 2011, following the tragic Fukushima Daiichi Nuclear accident, great attention has been devoted to the development of a new concept of nuclear fuel to improve the safety of nuclear reactors during normal operation, transient modes and under accident conditions [5–10]. A concept called “accident tolerant fuel (ATF)” indicates a strategy to prevent/limit the interaction of cladding material with water steam, or hydrogen embrittlement, and to reduce heat generation during cladding oxidation and increase “processing time” under accident conditions before re-flooding of the nuclear core [9,11,12].

The most crucial conditions for fuel claddings can occur in the case of a loss of coolant accident (LOCA) [1,10]. LOCA events can be caused by a breakup of the primary cooling system that results in the loss of pressure in the nuclear core and vaporization of the coolant. Under these conditions, the fuel temperature rises, thereby increasing the porosity

of the fuel and resulting in its fragmentation. The fuel cladding temperature also increases abruptly. When Zr-based (E110, E635, Zircalloys, M5, ZIRLO, etc.) claddings interact with water steam at a high temperature (above 800 °C), it causes oxidation and embrittlement by releasing additional heat due to the exothermic reaction:



Therefore, the development of ATF cladding material is desperately needed to enhance the robustness of LWRs in normal and possible accident conditions.

Nowadays, two main ATF strategies are considered. The first is to replace current cladding material with SiC_f/SiC composites [13–16], FeCrAl [17–21], molybdenum alloys [20,22–25] or Ni-based stainless steels [26]. Taking into account the duration and possible total costs for developing a new type of cladding material, this way is considered as a long-term strategy. The second ATF concept is the development of protective coatings on the surface of Zr fuel claddings [27,28]. Protective coatings should strongly improve corrosion and high-temperature (HT) oxidation resistance, wear-resistance and reduce hydrogen absorption of Zr-based alloys used in LWRs. Therefore, coating technology can be added to the technological process of nuclear fuel production that can be achieved in a short-term period. Despite the simplicity of this approach, a large number of possible factors (coating adhesion, thermal conductivity, thermal neutron cross-section, radiation resistance, mechanical properties [29]) can affect the behavior of coated Zr claddings in both normal and accident conditions. Currently, numerous studies are being performed to improve zirconium alloy performance by the deposition of metallic (Fe-based alloys, Cr, Cr-Al, Y, Ni-Cr, etc.), non-metallic (oxides, nitrides, carbides) or MAX-phase coatings [19,30–32]. Among a variety of coatings, the highest performance in LOCA scenarios belongs to materials which can produce oxide phases such as alumina, zirconia, chromia or silica [33–36].

This review emphasizes recent advances in protective coatings for ATF zirconium claddings. Section 2 introduces the Zr-based alloys and their behavior under normal and accident conditions. Section 3 presents different types of protective coatings for ATF concepts, while Section 4 elaborates on the mechanism of protection of selected coating types and provides several suggestions to develop Zr-based ATF claddings.

2. Zirconium-Based Alloys

Zirconium-based alloys have gained commercial acceptance based on their excellent properties and availability of metal in sufficient reserves and obtainable costs. Zirconium-alloy clad tubes were first developed by the United States Navy Nuclear Propulsion Program in the 1950s [36,37]. Nuclear-grade Zr-alloys consist of more than 95 percent Zr, and therefore possess characteristics close to those of pure Zr. Over decades, by optimization of elemental composition, the USA favored the Zr-Sn based alloy system while Russia, Canada and other countries developed an Zr-Nb based alloy system [10,38,39]. Zircalloys, ZIRLO, E-grades and M5 alloys will be discussed in this section considering their material composition and oxidation performance under accident conditions.

2.1. Zr-Sn and Zr-Nb Alloys

Unalloyed zirconium has poor corrosion resistance, resulting in high stresses and cracking of zirconium oxide and its spallation [40]. To decrease its corrosion rate under the normal operation conditions of a nuclear reactor, additional dopants were added into Zr, which should not strongly influence the neutron economy. Today, Zr is mainly alloyed with Sn and Nb. Moreover, O, Cr, Fe and Ni are also added in Zr alloys to improve their mechanical and functional properties. Table 1 presents various compositions of cladding materials currently used in the nuclear industry.

Table 1. Composition of Zirconium-alloys (wt.%) [41–46].

Alloys	Sn	Fe	Cr	Ni	Nb
Zircaloy-2	1.50	0.12	0.10	0.05	–
Zircaloy-4	1.50	0.20	0.10	–	–
ZIRLO	1.02	0.10	–	–	1.01
OPT-ZIRLO	0.66	0.11	–	–	1.04
M5	–	0.05	0.015	–	1.0
E110	–	–	–	–	0.95–1.05
E110 opt.	–	0.025–0.07	–	–	0.90–1.10
E110M	–	0.07–0.15	–	–	0.90–1.10
E125	–	–	–	–	2.20–2.60
E125 opt.	–	0.025–0.05	–	–	2.40–2.70
E635	1.1–1.3	0.30–0.40	–	–	2.40–1.05
E635M	0.70–0.90	0.30–0.40	–	–	0.70–0.90

Zircaloy 2 (Zry-2) belongs to the Zr-Sn system that shows a good balance between corrosion resistance and mechanical properties. The addition of Fe, Cr and Ni dopants improves the oxidation resistance of Zry-2 alloy. However, the presence of Ni caused high hydrogen uptake, so Zircaloy-4 (Zry-4) without Ni and increased Fe content was developed. Nowadays, two type of Zircaloys are used in the nuclear industry: Zry-2 in BWRs and Zry-4 in PWRs [41].

E110, E125 and E635 alloys belong to the Zr-Nb system used for structural components (fuel cladding, guide tubes, spacer grids, etc.) in the Russian VVER and RBMK reactors. These materials were developed from 1958 to 1971 and gained commercial acceptance in the 1980s, coupled with subsequent optimizations of their elemental compositions [45,46]. Despite the fact that both E110 and E635 alloys have been developed to possess creep resistance, high strength and resistance to irradiation growth, the E110 alloy has superior corrosion resistance in PWRs, while E635 provides high strength, resistance to creep and irradiation growth in BWRs [47,48]. E125 alloy is usually used for shroud pressure pipes of VVER and RBMK. E-series alloys are more vulnerable to breakaway corrosion than Zry-4, which results in higher oxidation rate and hydrogen uptake [7,49]. Thus, optimized modifications, such as E110opt., E110M, E125opt. and E635M, with Fe and O dopants, were developed to guarantee absolute assurance and integrity for use in the future generation of VVER (VVER-1200), which will operate at higher fuel burn-up [50,51].

ZIRLO alloy was designed by Westinghouse for PWR's fuel claddings. This alloy includes dopants of Sn, Fe, Nb and O. In 2004, an optimized version of the alloy (OPT ZIRLO) with reduced Sn (0.66 wt.%) and similar Fe (0.10 wt.%–0.11 wt.%) content was designed. OPT ZIRLO alloy has higher corrosion and creep resistance compared with ZIRLO, especially in Li-containing media [52].

M5 alloy has been in a commercial application since the 1990s as base material of the fuel claddings for PWRs. M5 and E110 alloys have similar basic compositions of Zr-1%Nb with controlled content of other dopants. The absence of Sn and an optimized heat treatment process of M5 alloy production result in very good corrosion resistance and mechanical properties under high temperature and irradiation conditions [53–55].

2.2. HT Oxidation Behavior of Zr-Based Alloys

LOCA, or reactivity-initiated accidents, can result in rapid oxidation of zirconium claddings, overheating and depressurization due to exothermic oxidation reaction (1). To estimate oxidation behavior of Zr alloys at HT, several experiments simulating severe accidents were performed. The results of these tests are presented below.

Malgin et al. studied HT (900–1250 °C) oxidation behavior of E110opt and E110M sponge-based Zr alloys in water steam [56]. The obtained results show similar oxidation kinetics of both alloys without breakaway effects. Yan et al. showed that the oxidation kinetics of sponge-based E110 alloy accelerates with increasing temperature, and a good correlation with the Cathcart–Pawel prediction model [57] was observed at 1200 °C

(Figure 1) [58]. The equivalent cladding reacted (ECR) parameter up to 17% of the initial cladding thickness was reached after 220–230 s at 1200 °C. Exceeding this value leads to a significant degradation of the mechanical properties of the fuel claddings, according to the criteria of the US Nuclear Regulatory Commission (NRC) [59].

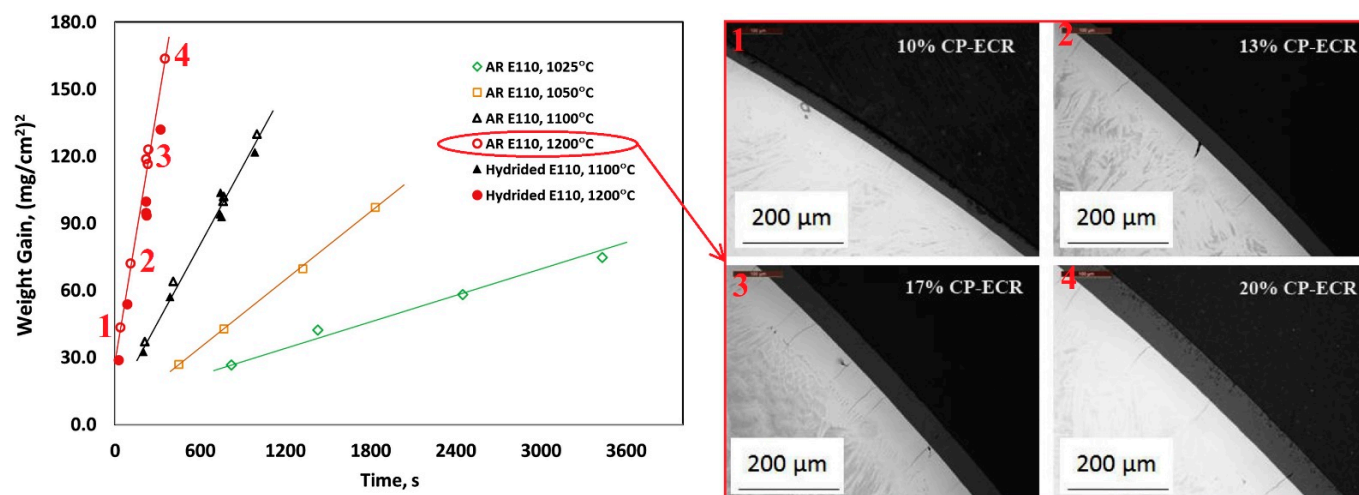


Figure 1. Parabolic oxidation curves of sponge-based E110 alloy in steam at 1025–1200 °C (left), and cross-section optical micrographs of the alloy after 1200 °C steam oxidation to 10%, 13%, 17% and 20% ECR (CP—Cathcart–Pawal, ECR—equivalent cladding reacted, AR—as-received). Reproduced from [58] with permission by Elsevier.

Le Saux et al. studied the breakaway oxidation of Zry-4 and M5 (Framatome) alloys in flowing steam at 950–1050 °C, as shown in Figure 2 [60]. The results concluded that the higher the temperature was, the greater the weight gain at which Zry-4 breakaway oxidation occurred in the ranges 8–11, 13–14 and 25–34 mg/cm², at 950–975, 1000 and 1025 °C, respectively. In contrast, M5 (Framatome) oxidized from both sides did not exhibit breakaway oxidation at temperatures from 950 to 1050 °C for up to 250 min (15,000 s). However, M5 breakaway oxidation occurred at 1025 °C beyond 15,000 s, with a weight gain of 15 mg/cm².

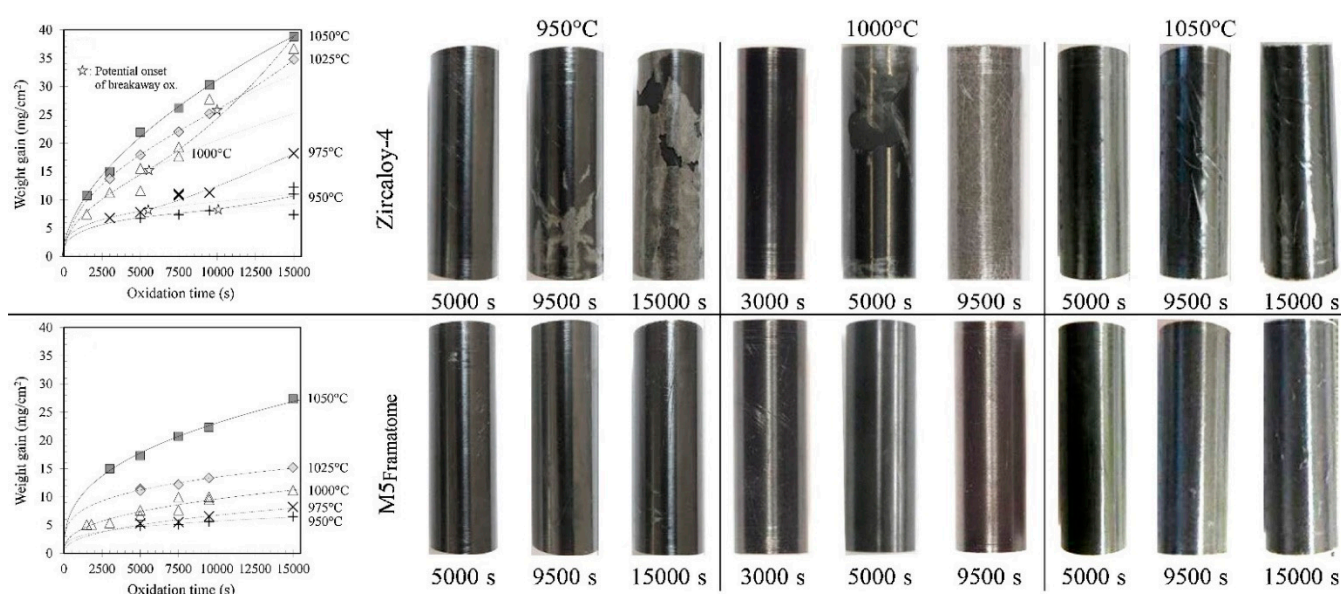


Figure 2. Post-quenching view of oxidized Zircaloy-4 and M5 (Framatome) cladding tube samples, oxidized in steam at 950–1050 °C. Reproduced from [60] with permission by Elsevier.

Steinbrueck et al. performed isothermal oxidation tests on Zry-4 alloy in a mixture of steam–nitrogen atmosphere by varying the volume fraction of the supplying gases at 600–1200 °C [61]. It was revealed that nitrogen significantly affected the oxidation kinetics due to formation and re-oxidation of ZrN to ZrO₂ near the metal/oxide interface. The re-oxidation process results in the loss of protective oxide scale due to the formation of microcracks as a result of high-volume expansion (approx. 48%) [62]. Thus, it is necessary to consider the effect of nitrogen, as it leads to the degradation of mechanical properties of zirconium alloy claddings and significantly increases oxidation kinetics and, therefore, the generation of hydrogen under accident conditions [63].

Since these results demonstrate low resistance of Zr-based alloys to HT oxidation under accident conditions, a new concept of nuclear material was developed to improve the safety of nuclear reactors [9].

3. Protective Coatings for ATF Claddings

Numerous studies have been performed to improve zirconium alloys' performance under both normal and accident conditions by the deposition of protective coatings [64–67]. Coated Zr alloys show enhanced corrosion and HT oxidation resistance; although reduced, relatively thin coatings are not influenced by the thermomechanical behavior of Zr-based claddings [73], the coatings should not noticeably change neutron absorption in LWRs [74] and heat transfer between the cladding and coolant [75].

Most published papers and reviews showed that ATF coatings should have at least one of Cr, Al or Si in their composition in order to enable the formation of a protective scale (Cr₂O₃, Al₂O₃, or SiO₂) [21,76–79]. Section 3 highlights recent developments in protective coatings for Zr-based alloys. A summary of the selected coatings and their performance under normal operational and accidental conditions is presented in Table 2.

3.1. Metallic Coatings on Zr-Based Alloys

3.1.1. Fe-Based Coatings

Currently, there are two major research institutes focusing on the development of FeCrAl coatings for nuclear fuel claddings. These are the Korea Atomic Energy Research Institute (KAERI) and the University of Illinois Urbana-Champaign (UIUC). Fe-based coatings on Zr necessitate a barrier layer between the coating and substrate to mitigate Zr-Fe eutectic formation at high temperatures [80]. Zhong et al. investigated the oxidation performance of FeCrAl coatings under HT steam conditions [81]. In this study, FeCrAl was deposited on Zry-2 alloy using magnetron sputtering. Based on the experimental results, 1 µm-thick FeCrAl coating prevented the oxidation of the Zry-2 substrate in steam at 700 °C up to 15 h, while a thin FeCrAl (0.3 µm) film did not protect the alloy. Furthermore, investigations performed under autoclave testing (20 days) in a simulated BWR environment demonstrated an adequate performance without the loss of coating integrity. Kim et al. investigated the surface-modified Zr cladding concept: an outer FeCrAl protective layer was chosen as a coating to enhance the oxidation/corrosion resistance of Zr alloy deposited by laser coating and arc ion implantation methods to increase the adhesion strength of the coating and the Zr alloy tubes [82]. The obtained samples demonstrate improved corrosion/oxidation performance, creep and irradiation resistance compared to commercial Zr claddings. Good radiation resistance was also observed for FeCrAl alloys under heavy ion irradiation [83]. There was no void formation or Cr-enriched phases in 10Cr and 13Cr FeCrAl alloys, and irradiation-induced defects only contributed to hardening. Dabney et al. showed that thick FeCrAl coatings obtained by cold spraying demonstrate high oxidation resistance during autoclave tests and HT oxidation in the air [84]. However, a fast diffusion of Fe from FeCrAl coating to Zr alloys caused a thick interlayer composed of (Fe,Cr)₂Zr, FeZr₃ and FeZr₂ Laves phases (Figure 3a,b) [85].

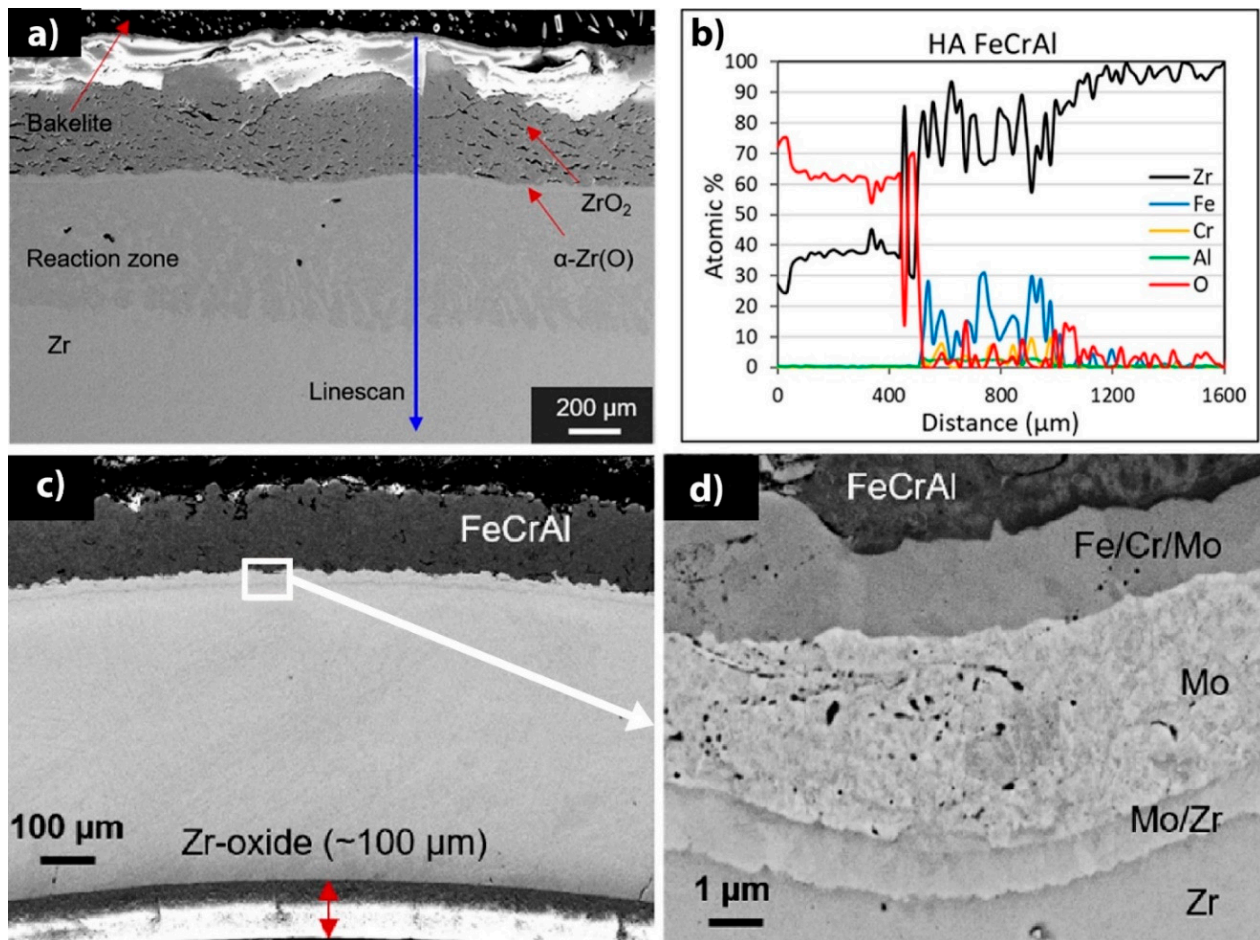


Figure 3. Cross-section SEM images after 1200 °C air oxidation: (a) FeCrAl-coated Zircaloy-4 and (b) corresponding EDS line scan; (c) FeCrAl/Mo coating and (d) magnified image of the FeCrAl/Mo/Zr interface. Reproduced from [84] with permission by Elsevier.

Park et al. investigated FeCrAl coatings deposited onto Zr substrates using cold spraying techniques [86]. For the FeCrAl/Zr system, a Mo layer was deposited between the FeCrAl coating and the Zr substrate to inhibit interdiffusion at high temperatures. As a result of mutual diffusion in the FeCrAl/Mo/Zr system, a complex multilayer structure was formed (Figure 3c,d). The FeCrAl coatings improved the oxidation resistance of the Zr alloy when exposed to a steam environment at 1200 °C. The ballooning behavior and mechanical properties of the coated samples studied under simulated LOCA conditions revealed higher burst temperatures, lower circumferential strain and smaller ruptures compared to the bare Zr. In addition, four-point bending and ring compression tests indicated a minimal increase in the maximum load and higher residual ductility of the coated Zr alloy, respectively [86].

3.1.2. Chromium-Based Coatings

Metallic Cr-based coatings are most promising in that they meet the basic requirements for ATF coating materials for fuel Zr claddings. Chromium has a high melting point, high corrosion resistance in water and steam due to a protective chromia scale, and a coefficient of thermal expansion similar to zirconium alloys. A wide variety of methods were implemented to deposit Cr coatings on Zr alloys such as magnetron sputtering [87], cathodic arc deposition [88], cold spraying [89], 3D laser cladding [90], electroplating [91], etc. The high potential of these coatings is also confirmed by the involvement of large industrial/research institutes such as CEA (France), VNIINM (Russia), KIT (Germany)

and others. Several full-scale tests with Cr-coated Zr claddings with UO_2 fuel in nuclear reactors are being performed at present.

Good protective properties of Cr coatings were demonstrated under normal operation conditions: autoclave testing in PWR and BWR simulated medium [65–67,92]. Wei et al. showed high corrosion resistance in Cr-coated Zry-4 alloy in both H_3BO_3 -LiOH and dissolved oxygen containing water [67], showing only 50–100 nm stable Cr_2O_3 scale after a 3000 h autoclave test. Chromium coatings deposited on Zry-4 alloy exhibited promising performance under steady-state, power ramp and LOCA transient conditions [93,94]. Brachet et al. showed good protective properties of a 5–12 μm thick Cr coating under steam oxidation at 1200 °C (Figure 4) [87]. It was demonstrated that the coating enhanced the oxidation resistance of the alloy and ensured the integrity of the cladding for a longer oxidation time (approx. 10 times longer than current LOCA criteria). Ma et al. showed that Cr coatings could protect Zr-1Nb alloy from HT steam oxidation at 1200 and 1300 °C (Figure 5) [95]. It was shown that the thickness of the formed Cr_2O_3 and residual Cr layers depends on oxidation time, which is probably due to the combined effect of the ongoing redox reactions between chromium oxide and zirconium, also observed by Han et al. [96].

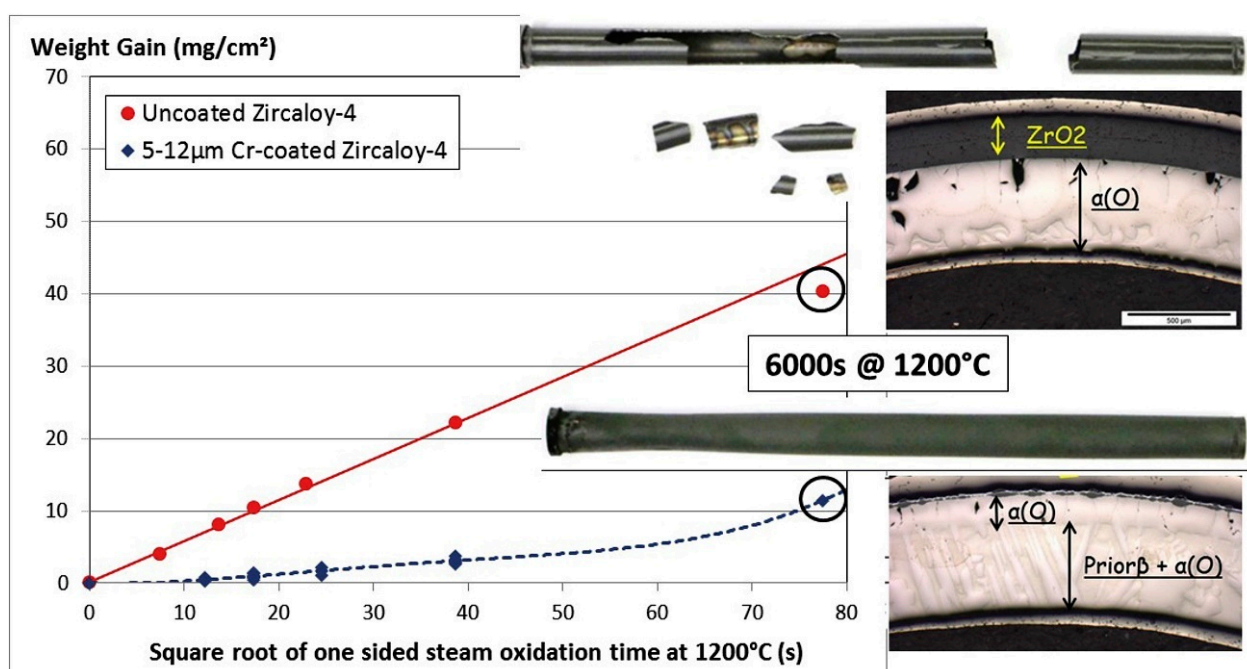


Figure 4. Optical images and weight gain evolution of uncoated and Cr-coated (5–12 μm) Zry-4 alloy during steam oxidation at 1200 °C. Reproduced from [87] with permission by Elsevier.

Results of mechanical tests under ambient and elevated (400 °C) temperatures showed no significant difference between the Cr-coated and the uncoated Zr claddings [65,90,97]. Kim et al. investigated the mechanical behavior of Zry-4 alloy with 3D laser-coated Cr coatings (80–120 μm) under ring compression and tensile tests [90]. The results indicate good adhesion and no defects in the Cr coatings up to 4% strain. The generation of cracks occurred at 6% strain without coating spallation or peeling. Ribis et al. analyzed the atomic-scale structure of the Cr/Zry-4 interface where the Cr coating was deposited using PVD method [98]. It was found that a thin layer of Laves $\text{Zr}(\text{Cr},\text{Fe})_2$ phase with C14 and C15 polytypes was formed at the interface, while the coherent boundaries ensured good adhesion of the coating.

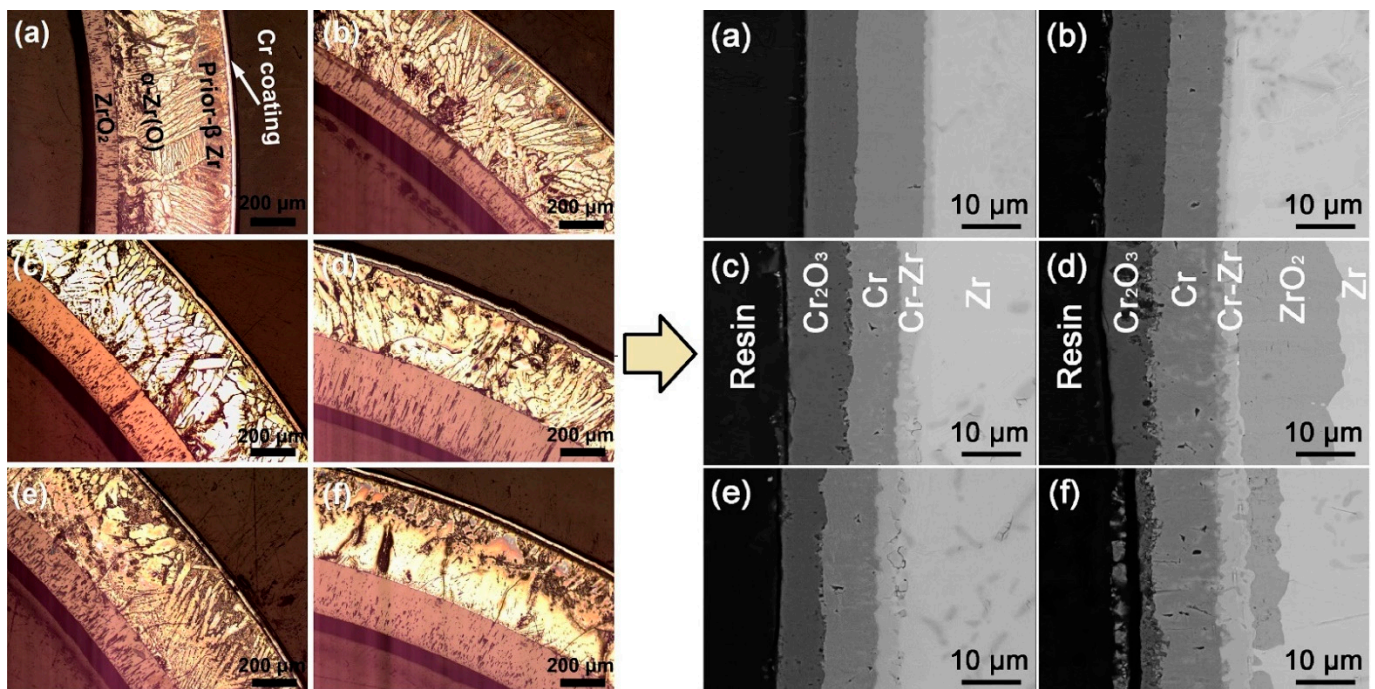


Figure 5. Optical and SEM images of Cr-coated zirconium alloy cladding after high-temperature steam oxidation at 1200 °C for 0.5 h (a), 1 h (b), 2 h (c), 4 h (d), and 1300 °C for 0.5 h (e) and 1 h (f). Reproduced from [95].

The adhesion behavior of Cr coatings was also affected by oxidation and diffusion processes at the coating/alloy interface [72]. Jiang et al. performed a comparative analysis of cracking resistance of multi-arc ion plated Cr and CrN coatings on Zry-4 alloy under tensile loading [99]. It was revealed that Cr coatings exhibit a brittle-to-ductile transition under thermomechanical loading, which results in their better cracking resistance compared to CrN coatings.

Several studies presented a good radiation resistance of chromium coatings under ion irradiation [100–102]. The stabilization of C14 and disappearance of C15 polytypes in the Cr/Zry-4 samples due to continuous incoming Fe flux were found during 20 MeV Kr⁺ irradiation at 400 °C. Despite this, the samples retained their adhesion and microstructure stability after ion irradiation [100]. An acceptable swelling of ~1.6% was observed at an irradiation temperature of 500 °C under 1.4 MeV heavy ion radiation up to 25 dpa [101]. This is twice lower than the allowable swelling value (~5%) for reactor materials.

Cr-Al alloy coatings show better oxidation resistance than pure chromium [80,103,104]. However, a more complex and heterogeneous structure of the oxide layers forms after oxidation [105], which requires more detailed studies under long-term HT steam oxidation, as well as B-DBA conditions. Ni-Cr coatings exhibit better ductility than pure Cr coatings but, at high temperatures, they show lower oxidation resistance and rapid diffusion of Ni inside the zirconium alloy occurs [106,107].

3.1.3. Yttrium-Based Coatings

The resistance of yttrium to oxidation, as well as the formation of stable protective yttrium oxides at very high temperatures, made it very attractive for study. Sridharan et al. investigated surface modified Y-coated Zry-2 alloy and observed a decrease in the oxidation rate in supercritical water at 400 °C for 7 days (168 h) [108]. Kim et al. investigated the surface modification of 2 mm-thick Zry-4 alloy by deposition of Y₂O₃ (10 μm) using a laser beam scan method to produce an oxide dispersion strengthening (ODS) treatment [109]. It has been shown that the yield strength of Zry-4 with the ODS layer was 65% higher compared to uncoated alloy at 500 °C, therefore enhancing high-temperature strength to defeat the ballooning behavior of fuel cladding during an accident event [110]. However,

the limited research on these types of coatings does not allow us to confirm the feasibility of their use as ATF materials.

3.1.4. HEAs Coatings

High entropy alloys (HEA), also called multi-principal component alloys, are solid solutions of at least four elements in near equimolar ratios [111,112]. HEAs demonstrate a wide range of outstanding properties, such as high thermal stability, corrosion resistance and radiation damage tolerance [113,114]. Zhang et al. investigated corrosion behavior of a 3 μm -thick AlCrMoNbZr HEA coating deposited on an N36 alloy (Zr-1Sn-1Nb-0.3Fe) in static water at 360 °C and 18.7 MPa for 30 days [115]. It was reported that the oxidation resistance of the N36 alloy increased threefold due to multiphase oxide phases ($\text{Nb}_2\text{Zr}_6\text{O}_{17}$, ZrO_2 and Cr_2O_3) formed at the surface. A multilayer AlCrMoNbZr/(AlCrMoNbZr)N coating can be beneficial for preventing Al migration and boehmite phase formation during autoclave corrosion of an AlCrMoNbZr alloy [116]. The multilayer AlCrMoNbZr/(AlCrMoNbZr)N coating with the layer step of 50 nm demonstrated better protective properties compared to 5/5 nm and 10/10 nm multilayers and single-layer AlCrMoNbZr (Figure 6) [117]. Despite the potential application of HEAs as ATF materials for fuel claddings [118–121], their application as protective coatings is challenging due to possible low temperature eutectics, with Zr alloys and complex oxide scales formed after HT oxidation.

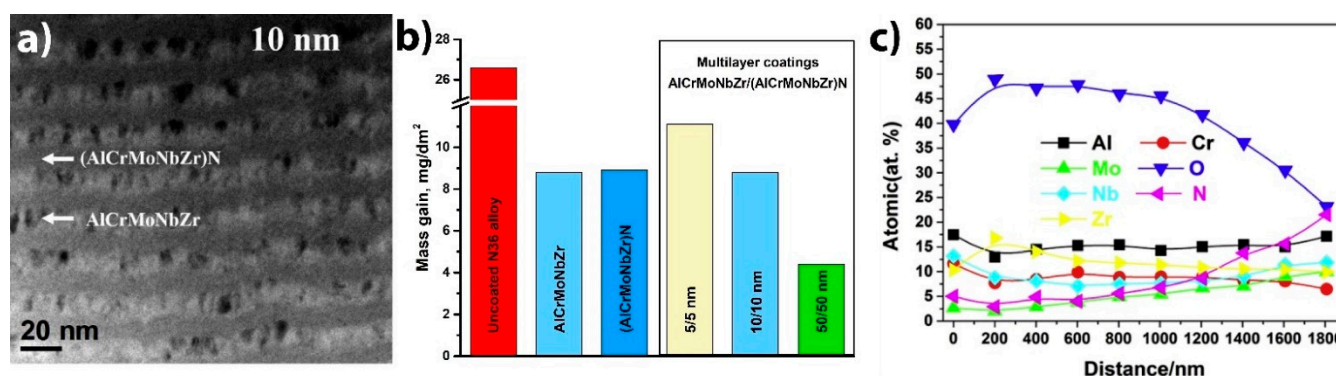


Figure 6. Multilayer AlCrMoNbZr/(AlCrMoNbZr)N HEA coatings: (a) cross section TEM image of 10/10 nm coating; (b) mass gains for HEA-coated N36 zirconium alloy after an autoclave test at 360 °C, 18.7 MPa for 30 days; (c) depth distribution of elements in 50/50 nm HEA coating after the autoclave test. Reproduced from [117] with permission by Elsevier.

3.2. Non-Metallic Coatings on Zr-Based Alloys

3.2.1. Nitride Coatings

There are several research groups working on the development of nitride coatings for nuclear fuel Zr claddings. Khatkhatay et al. deposited TiN and $\text{Ti}_{0.35}\text{Al}_{0.65}\text{N}$ coatings on Zry-4 substrates using pulsed laser deposition, and exposed them to supercritical water conditions for 48 h at a temperature of 500 °C and a pressure of 25 MPa [122]. The coated tubes were remarkably intact after exposure, while uncoated tubes demonstrated severe oxidation and breakaway corrosion. The TiN coatings also reduce the hydrogenation of Zr alloys [123]. However, nanocrystalline TiN coatings can dissociate under energetic particle bombardment, forming Ti-enriched zones with low oxidation resistance [124]. Despite good diffusion barrier properties of TiN coatings [125], they are considered less as a protective coating or barrier interlayer because of their large coefficient of thermal expansion (CTE) difference with Zr and possible cracking during thermal cycling [126]. Alat et al. studied the corrosion resistance of TiAlN and TiN coatings deposited on ZIRLO substrates by cathodic arc physical vapor deposition [127,128]. The corrosion tests were implemented in static pure water at 360 °C and 18.7 MPa for 72 h. After the tests, a very low

weight gain between 1–5 mg/dm² was observed, whereas the uncoated ZIRLO samples showed an average weight gain of 14.4 mg/dm². However, aluminum depletion in a high-temperature water environment results in the formation of a boehmite phase that degrades the corrosion resistance of TiAlN coatings (Figure 7). To eliminate boehmite formation, the deposition of an outer TiN layer or multilayer approach based on TiN/TiAlN coating can be effective [128,129].

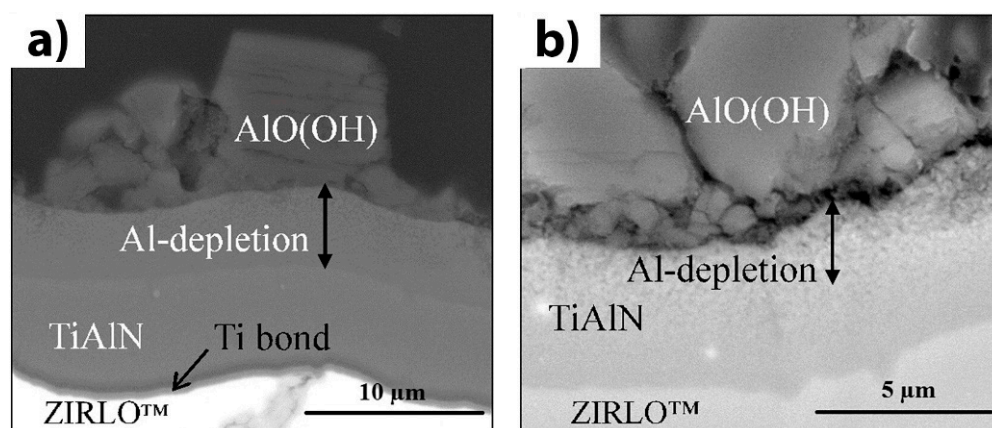


Figure 7. Cross-section SEM images of TiAlN/Ti/ZIRLO™ after autoclave testing at 360 °C for 72 h: (a) secondary electron mode, and (b) backscattered electron mode. Reproduced from [127] with permission by Elsevier.

Daub et al. provided comparative analyses on corrosion resistance of 2–4 μm-thick CrN-, TiAlN- and AlCrN-coated Zry-4 alloy [130,131]. It was shown that a CrN coating demonstrates better overall performance in both aqueous and steam environments, as well as twice-reduced hydrogen ingress. Meng et al. showed the high resistance of a 13 μm-thick CrN coating deposited on a Zr-702 alloy in the air up to 1160 °C (Figure 8) [132]. Krejčí et al. demonstrated cracking and local failures of CrN coatings after HT steam oxidation at 1200 °C for 30 min [133]. It was indicated that the cracking was caused by partial decomposition of CrN to Cr₂N at high temperatures (typically below 850 °C) [134].

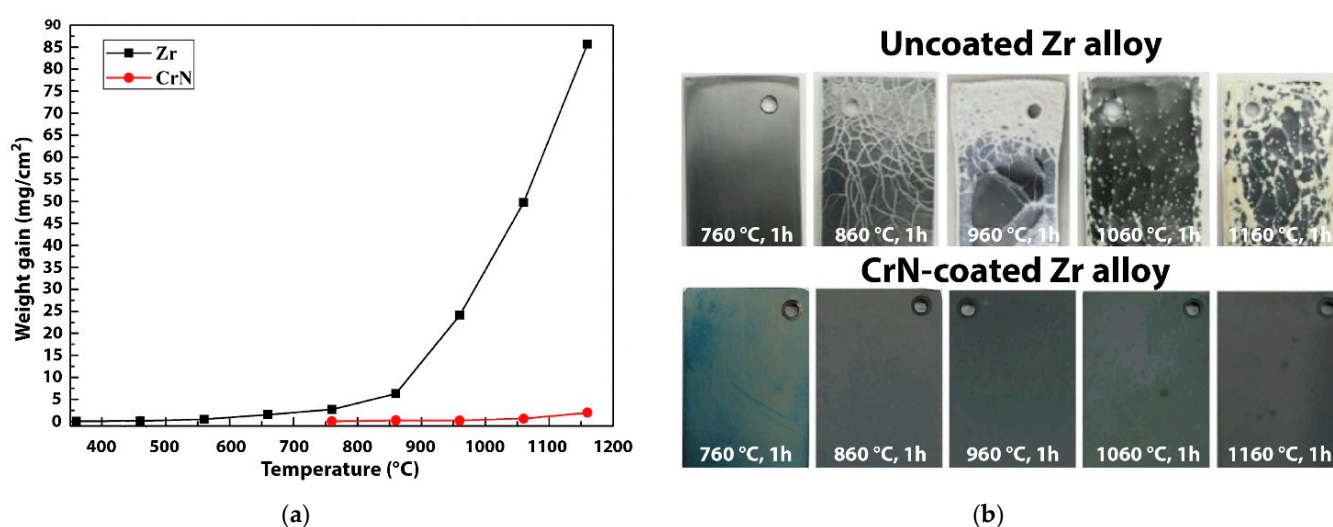


Figure 8. Weight gain of uncoated and CrN-coated Zr alloys as the function of oxidation temperature in the air (a), and the appearance of the samples after the oxidation tests (b). Reproduced from [132] with permission by Elsevier.

3.2.2. Zirconium Silicide Coatings

Zirconium silicides have high thermal conductivity and favorable mechanical properties [135]. Yeom et al. studied the oxidation behavior of Zr_2Si , $ZrSi$ and $ZrSi_2$ coatings deposited on a Zry-4 alloy by magnetron sputtering [136]. Thicker ($3.9\text{ }\mu\text{m}$) $ZrSi_2$ coating exhibited oxidation resistance almost two orders of magnitude higher compared to uncoated Zry-4 in $700\text{ }^\circ\text{C}$ air for 20 h. The thicknesses of the oxide layers were 7 and $20\text{ }\mu\text{m}$ for coated Zry-4 at $1000\text{ }^\circ\text{C}$ (1 h) and $1200\text{ }^\circ\text{C}$ (10 min) steam, respectively. No cracking or spallation was observed after three cycles of water quenching from $700\text{ }^\circ\text{C}$. However, the brittle nature of silicide coatings and coating volatilization under autoclave testing limit their application for ATF [137].

3.2.3. Carbide Coatings

Silicon carbide is a promising material for ATF Zr claddings since it has a high melting point, low chemical reactivity, superior oxidation resistance at high temperatures and a lower thermal neutron cross-section than Zr-based alloys [138]. SiC coatings deposited on a Zry-4 alloy using co-sputtering of SiC and Si targets demonstrate enhanced oxidation resistance in $900\text{ }^\circ\text{C}$ steam due to the formation of a protective silica layer [139]. SiC coatings obtained by magnetron sputtering also reduce the hydrogenation of zirconium alloys under normal operation temperatures [140,141]. The effect of deposition parameters on the mechanical properties of SiC coatings deposited on Zircaloy-4 substrate by magnetron sputtering was shown in [142]. Al-Olayyan et al. showed better adhesion of SiC coating on rough surfaces of Zry-4 alloy, which resulted in higher corrosion resistance [143]. Nevertheless, unstable oxide growth and coating volatilization during autoclave corrosion tests must be considered carefully when designing SiC-based coatings for LWRs [144].

Zr-Al-C coatings obtained on Zry-4 alloy by magnetron sputtering demonstrated poor protective properties during oxidation in steam at temperatures beyond $800\text{ }^\circ\text{C}$ due to formation of ZrO_2 and Al_2O_3 oxides scales [145]. Michau et al. studied the protective properties of Cr-based carbide (CrC , $CrSiC$) coatings deposited on the inner surface of Zr cladding tubes using DLI-MOCVD [146]. Good adhesion and better oxidation resistance of amorphous Cr_xC_y coating in air and steam at $1200\text{ }^\circ\text{C}$ were shown (Figure 9), while the addition of Si was ineffective in improving oxidation resistance of chromium carbide coatings. It was also shown that an optimized DLI-MOCVD process can be successfully used to deposit CrC_x coatings inside Zr cladding tubes 1 m in length [147,148].

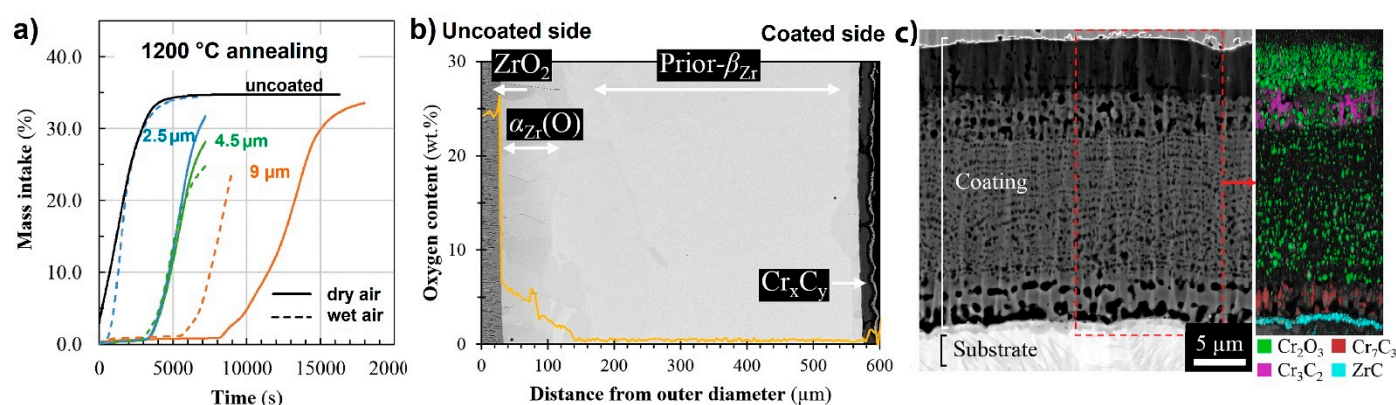


Figure 9. Mass gains measured by TGA of uncoated and Cr_xC_y -coated Zircaloy-4 under air oxidation isothermal air oxidation at $1200\text{ }^\circ\text{C}$ (a); BSE SEM image and oxygen profiles of Cr_xC_y -coated clad segment after oxidation in steam at $1200\text{ }^\circ\text{C}$ for 10 min, followed by water quenching (b); and the detailed SEM + EBSD image of the inner surface of Cr_xC_y -coated clad segment after the oxidation test (c). Reproduced from [146] with permission by Elsevier.

Jin et al. deposited $75Cr_3C_2$ - $25NiCr$ (wt.%) on a Zr-2.5Nb alloy using a high velocity oxygen fuel (HVOF) technique and showed improved oxidation resistance in air and steam at 700 – $1000\text{ }^\circ\text{C}$ [107]. However, the coated samples showed poor corrosion resistance

in supercritical water at 400 °C and 10.3 MPa, caused by a bimetallic effect (this coating can build up bimetallic couple with the Zr-2.5Nb alloy, resulting in the acceleration of the corrosion rate). Yang et al. demonstrated high oxidation resistance of 120 µm-thick HVOF Cr₃C₂-NiCr coating at 1200 °C in steam for 1 h due to the formation of a dense chromia scale [149]. However, the high coating thickness and heterogeneous/porous microstructure formed by the HVOF method may limit the usefulness of such coatings for ATF Zr claddings.

3.2.4. MAX-Phase Coatings

MAX phases are layered hexagonal carbides and nitrides referenced to the general formula $M_{n+1}AX_n$, (MAX), where “n” ranges between 1 and 4, “M” represents a transition metal (Sc, Ti, V, Cr, etc.), “A” is an A-group (mainly III_A and IV_A, or groups 13 and 14) element and “X” is either C and/or N [150,151]. MAX phase materials exhibit excellent properties of both metals and ceramics such as high electrical and thermal conductivity, high melting points and excellent oxidation resistance [152,153].

Alumina-forming MAX phases demonstrate superior oxidation resistance at high temperatures and exhibit self-healing ability [154]. Li et al. investigated high-temperature oxidation resistance of 12 µm-thick Ti₂AlC coating on ZIRLO alloy in pure steam at 1000–1200 °C [155]. The coating remains intact and demonstrates good protective properties up to 1200 °C during 5 min oxidation time. The improved oxidation resistance was due to the dense columnar-free microstructure of Ti₂AlC coating and triple oxide scale α -Al₂O₃ + rutile-TiO₂/α-Al₂O₃/TiO₂. Maier et al. showed the oxidation resistance of cold sprayed Ti₂AlC coating (90 µm) in Ar/steam mixture at 1005 °C for 20 min [156]. The Ti₂AlC coating protected the Zry-4 alloy from oxidation and had high hardness and wear resistance. Thinner Ti₂AlC/TiC coatings (5/0.5 µm) deposited by magnetron sputtering demonstrate high oxidation resistance in steam at 800 °C, forming a triple-layered scale (θ-Al₂O₃ + TiO₂/θ-Al₂O₃/TiO₂) [157]. It was also shown that the TiC barrier layer mitigates the inward diffusion of Al into the Zry-4 alloy. However, rapid oxidation at 1000 °C resulted in cracking and spallation of the Ti₂AlC coatings.

The oxidation resistance of Ti-Al-C and Cr-Al-C coatings deposited by magnetron sputtering on ZIRLO alloy was investigated in [158]. Results of the autoclave test at 360 °C and 18.6 MPa showed poor protective properties of Ti-Al-C coatings due to the formation of multiple oxide scale and hydroxide phases. The Cr₂AlC coating demonstrates better oxidation performance; however, partial spallation and formation of volatilized AlOOH was also revealed. Tang et al. showed the excellent oxidation resistance and self-healing ability of thin Cr₂AlC coatings in steam at 1000 °C (Figure 10) [159].

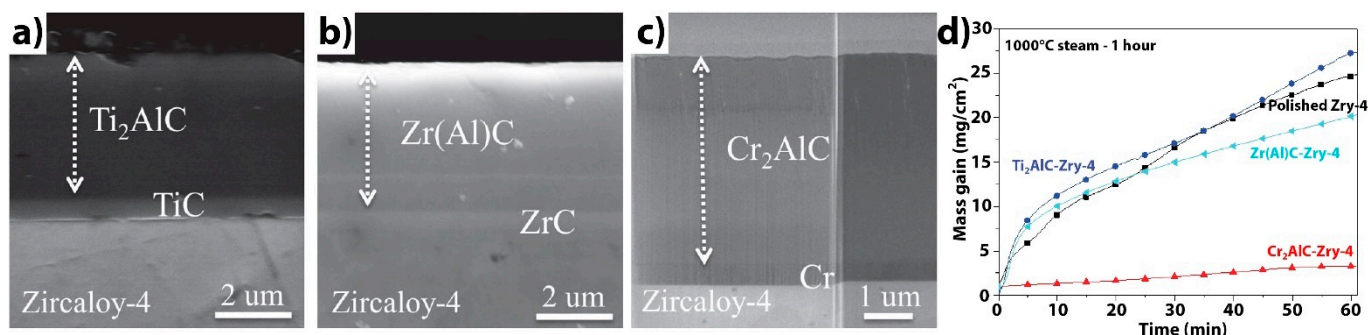


Figure 10. Cross-section images of three types of MAX-phase coatings with barrier layers on Zircaloy-4 after annealing: (a) Ti₂AlC, (b) Zr(Al)C, (c) Cr₂AlC, and their oxidation kinetics in 1000 °C steam (d). Reproduced from [159] with permission from the authors.

Imtyazuddin et al. analyzed the radiation resistance of magnetron sputtered Cr₂AlC films under 320 keV Xe ions at 300 and 623 K [160]. It was found that Cr₂AlC films are amorphized at room temperature even at low doses; however, no amorphous phase was

found up to 90 dpa at 623 K, indicating good radiation tolerance at elevated temperatures (Figure 11). Furthermore, both Ti_2AlC and Cr_2AlC coatings reduce hydrogen uptake effectively [161]. Wang et al. also demonstrated good oxidation resistance of 10 μm -thick Cr_2AlC coatings in air at 1100 $^\circ\text{C}$ [162].

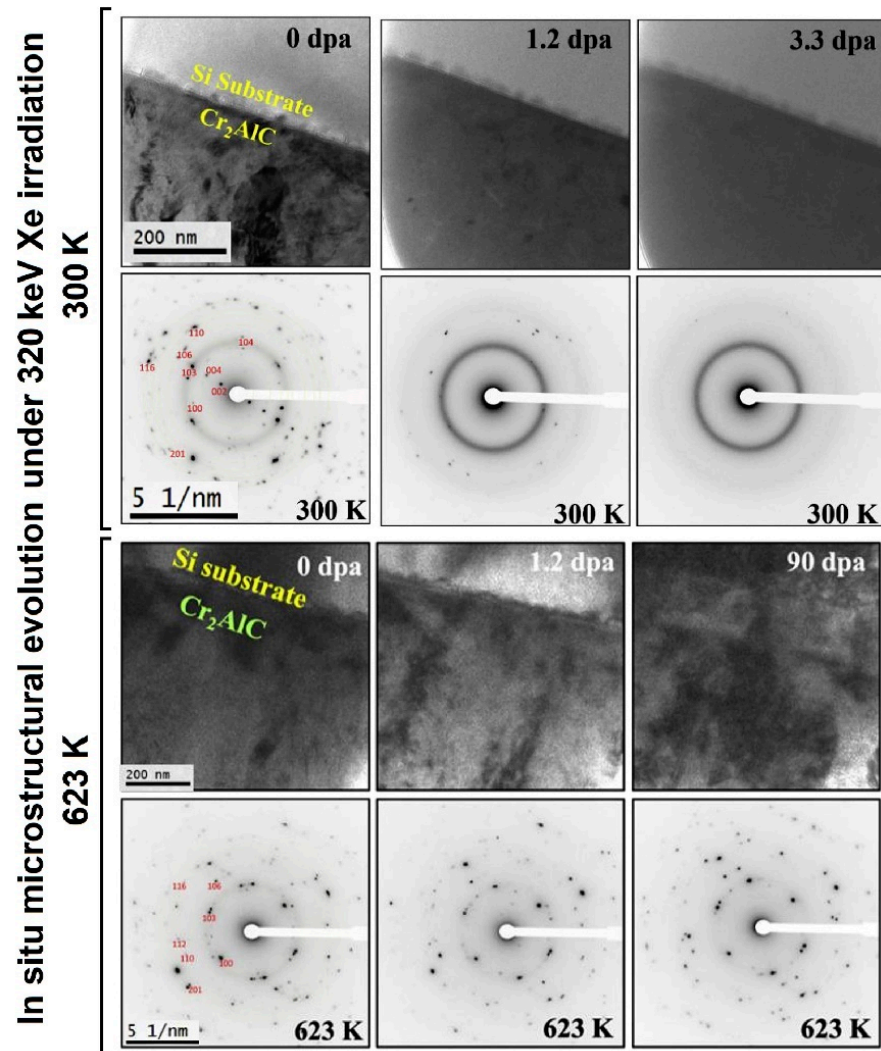


Figure 11. Evolution of microstructure of magnetron-deposited Cr_2AlC thin film under 320 keV Xe irradiation at 300 and 623 K. Reproduced from [160] with permission by Elsevier.

A literature review indicates the rapid diffusion of “A” element from the MAX phases into the Zr alloys with the formation of an interdiffusion layer, thereby decreasing the protective properties of the coating. Thus, various diffusion barrier layers between the coating and the substrate should be considered when developing protective coatings for ATF based on MAX-phases.

4. Mechanism of Protection

Coating methods, materials and deposition parameters play significant roles in oxidation resistance of protective coatings. The key protection mechanism involves the formation of a stable oxide layer on the coating surface with a low oxidation rate. Stable and well-studied oxides include alumina (Al_2O_3), silica (SiO_2) and chromia (Cr_2O_3). Therefore, further discussion will focus mainly on the coatings forming these oxides, especially on chromium-based coatings. One of the important problems considered is the volatilization/sublimation of oxides in water and steam under normal operation and

DBA conditions [163]. Among the indicated oxides, chromia is the only stable one that is slowly volatilized/sublimated during autoclave and LOCA conditions [19]. The sublimation rate of alumina and silica is not expected to be a problem at temperatures below 1300 °C; however, noticeable volatilization was shown after autoclave tests in a simulated PWR medium [164]. In addition, the protective coating, as well as the growing oxide layer, should have a dense microstructure to reduce the diffusion of oxygen and hydrogen (generated from oxidation reaction) along the grain boundaries of the coating.

Another serious issue is interdiffusion at the interface of the protective coating and the alloy. Interdiffusion is observed mainly for metallic coatings due to higher diffusion coefficients of species in metals compared to ceramics. Thus, during oxidation of metallic coatings, the coating can be consumed by oxide growth and formation of the interdiffusion layer. Interdiffusion is also aggravated by the fact that eutectic phases with low melting points can form, especially in the case of B-DBA conditions. Therefore, the rates and mechanisms of interdiffusion for each type of coating, as well as methods to inhibit the diffusion, should be revealed and considered in detail.

4.1. Microstructure and Thickness of the Coatings

It is well known that not only the composition of the coatings but also their microstructure and thickness play an important role in their oxidation resistance.

Despite little research, the influence of coating thickness on oxidation resistance has been well studied. Brachet et al. performed comparative analysis of the mass gains for Zry-4 alloy with 1–12 µm-thick PVD Cr coatings after HT steam oxidation at 1100 °C for 850 s [87]. The results demonstrated a reduction of the mass gain of Cr-coated samples from 6.5 mg/cm² to <1 mg/cm², with increasing coating thickness. Kashkarov et al. investigated the oxidation kinetics of Cr-coated E110 alloy in 1200 °C steam for 10 min, depending on coating thickness and microstructure [165]. It was shown that the weight gain of Cr-coated samples was reduced from 22.1 to 4.1 mg/cm², as coating thickness increased from 4.5 to 9.0 µm. A similar observation was shown for a E110 alloy, with magnetron-deposited Cr coatings after HT air oxidation tests at 1100–1200 °C [72].

Protective coatings can provide a significant additional delay before oxidation, as HT becomes too detrimental to the mechanical integrity of the claddings. Accelerated oxidation kinetics of Cr-coated Zr alloys was observed after a transition period, whereby the coating state changed from protective to non-protective (Figure 12a) [166]. The duration of the protective period, as well as transition time, are mainly dependent on coating thickness (Figure 12b).

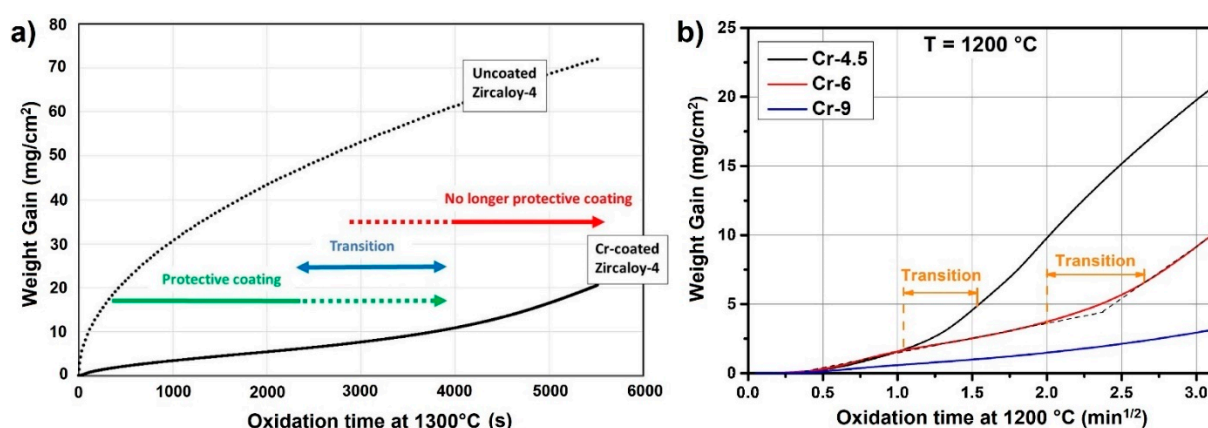


Figure 12. Mass gain evolution measured by TGA: (a) 10–15 µm Cr-coated Zry-4 alloy in helium–oxygen mixture at 1300 °C (reproduced from [166] with permission by Elsevier); (b) 4.5–9 µm Cr-coated E110 alloy in steam at 1200 °C (reproduced from [165] with permission by Elsevier).

The mechanism of HT steam oxidation of Cr-coated zirconium alloys was suggested and described in [166]. The oxidation process can be divided into three stages characterized by protective, transition and non-protective behavior (Figure 13). During the protective stage, the oxidation rate is controlled by the growth of the protective Cr_2O_3 outer layer. At the same time, inward diffusion of residual Cr into the alloy results in the formation of a Cr_2Zr interlayer at the interface, while the outward diffusion of Zr occurs along the grain boundaries of the coating. It is also worth noting that oxygen can diffuse along the grain boundaries of the coating to the zirconium alloy, especially in the case of columnar or porous microstructure of the coatings. The oxidation rate gradually increases during the transition stage, which is probably caused by the formation of a zirconia network at the grain boundaries, enhancing oxygen transport to the alloy. Han et al. and Ma et al. pointed out a reduction-oxidation mechanism between Zr and Cr_2O_3 [95,96], which can lead to partial reduction of Cr_2O_3 , thereby slowing down the growth rate of the outer chromia scale. Along with the growth of the outer Cr_2O_3 layer, the continuous oxygen ingress into the Zr alloy leads to the formation of an oxygen-stabilized α -Zr(O) phase beneath the coating, and then the growth of ZrO_2 due to subsequent oxidation of α -Zr(O) and ZrCr_2 phases. During oxidation, the ZrCr_2 interlayer can be transformed into metallic Cr and zirconia grains. At the third stage, the highly oxidized coating demonstrates non-protective behavior and the oxidation rate is mainly controlled by the growth of the zirconia layer.

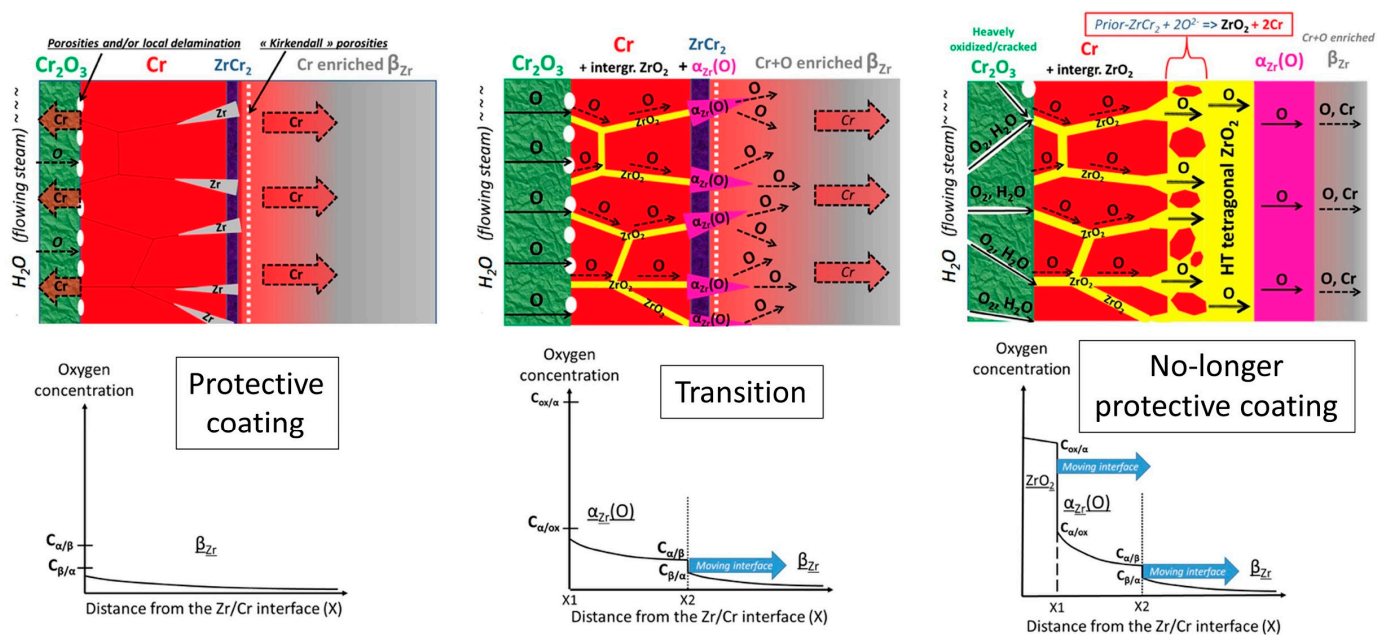


Figure 13. Schematic overview of the HT steam oxidation process of Cr-coated zirconium-based alloy. Replotted from [166] with permission by Elsevier.

An analysis of autoclave and high-temperature oxidation tests showed that chromium coatings must be at least 10 μm -thick to provide long-term protection (see Table 2). However, the thickness of protective coatings on Zr-based claddings should be limited to avoid a significant impact on the neutron transport in LWRs. For example, for Cr coatings, thickness should not exceed 30 μm , so that the reduction of fuel cycle life would be limited to 1% [167].

As long as the Cr coating is intact/protective, the microstructure of the Cr coatings is the key characteristic in normal operation and accident conditions [165,168–170]. It has been shown that the activation energy of oxidation is higher for dense Cr coatings compared to columnar ones. It was found that pre-annealing of the Cr coatings on Zircaloy-4 at 700 and 800 $^{\circ}\text{C}$ for 2 h increases the resistance of the coating to oxidation due to an increase in grain size (recrystallization) [166]. The columnar structure of coatings is undesirable,

as it significantly decreases their corrosion resistance due to the rapid diffusion of oxygen along the grain boundaries down to the Zr alloy. Thus, it is necessary to maintain an optimal balance in which the coating exhibits high corrosion resistance and acceptable mechanical properties to reduce wear and mechanical damage of coatings during assembly, transportation and operation of fuel element claddings.

To obtain coatings with a dense and uniform microstructure, deposition technology should be optimized to create special conditions for coating growth. For example, during magnetron sputtering, the ratio of substrate temperature to the melting point of coating material is considered a key criterion [171,172]. To arrive at these conditions, preliminary heating or substrate biasing can be used. Moreover, a perspective approach uses sputtering technologies with a high ion-to-neutral ratio, as present in a magnetron with a closed magnetic field or high power [173,174].

Changes in the composition and crystalline structure of Cr-based coatings affect their corrosion resistance and mechanisms. Ougier et al. studied the air oxidation behavior of Cr-Al-C and annealed Cr₂AlC MAX-phase coatings deposited using an HiPIMS technique [175]. It was found that mixed Al₂O₃ and Cr₂O₃ phases form at the top surface of the as-deposited Cr-Al-C coating, while a dense and continuous Al₂O₃ layer forms on the Cr₂AlC coating at the initial stage of the oxidation test (15–30 min at 1200 °C). However, a porous Cr₇C₃ interlayer is formed during continuous oxidation due to the outward diffusion of Al and Cr, and the interdiffusion of Cr, Al and C into Zr alloy. Liu et al. showed the effect of Si addition on oxidation resistance of CrAlN coating in steam at 1000 and 1200 °C [176]. A bilayered structure consisting of outer Cr-rich and inner Al-rich mixed Cr and Al oxides layers was formed after oxidation at 1200 °C. It was also found that CrAlN coatings have better oxidation resistance compared to CrAlSiN ones because the latter coatings are easily cracked in HT steam due to the formation of nanosized Si₃N₄ and SiO₂ grains.

Table 2. Summary of selected protective coatings for Zr-based alloys.

Coating/Substrate	Deposition Method	Microstructure	Thickness, μm	Oxidation Conditions	WG, mg/cm^2	Comments	Refs.
Cr/Zry-4	PVD	Dense	15–20	PWR medium, 360 °C, 415 °C, 10 MPa, 200 days	0.05	-Excellent corrosion resistance under autoclave testing; -High oxidation resistance in steam under DBA and for short period B-DBA conditions; -Enhanced post-quench ductility compared to uncoated alloy; -Reduced hydrogen pick-up under HT steam.	[92]
				Steam 1200 °C, 1500 s	2.60		
				3. Steam, 1300 °C, 5600 s	21.20		
Cr/E110	Dual MS	Dense voids-free	3.1	Air, 1100 °C, 20 min	2.86	-Hot and cooled target magnetron sputtering produce Cr coatings with different microstructures; -Thicker Cr coatings demonstrate higher oxidation resistance; -Magnetron sputtering techniques with higher energy per one deposited atom produces better oxidation resistant coating; -Coating adhesion affected by substrate oxidation and interface reactions; -Transition time into non-protective behavior increases with coating thickness; -Interdiffusion of Cr and Zr significantly affects the oxidation kinetics.	[72], [165]
			4.5	Steam, 10 min: 900 °C	0.33		
				1050 °C	1.40		
	Hot target MS	Columnar	6.0	1200 °C	22.90		
				Steam, 10 min: 900 °C	0.52		
				1050 °C	1.60		
			9.0	1200 °C	12.6		
				Steam, 10 min 900 °C	0.45		
				1050 °C	1.00		
Cr/Zry-4	CAPVD	Columnar	20	1200 °C	4.10		
				PWR medium, 360 °C, 18.6 MPa, 2000 h	0.048	-Cr-coated alloy corrodes much slower than Zry-4 alloy in both H_3BO_3 -LiOH and dissolved oxygen containing water; -Bubbles are observed at the surface of the coated samples after oxidation at 1200 °C.	[67]
				BWR medium, 360 °C, 18.6 MPa, 3000 h	0.035		
Cr/Zry-4	PVD/HiPIMS	Columnar Dense/Multilayered Dense	1	Air, 800–1200 °C, 1 h	–	-Cr coatings show better oxidation performance than nitrides (TiN, CrN, TiN/AlTiN, CrN/AlTiN) and metallic alloy (NbV, NbCrTi, Cr/NbCrTi) coatings; -Cr-based coatings exhibited good compromise between nominal corrosion resistance and coating adhesion, good fretting wear resistance, as well as improved HT steam oxidation resistance at DBA and slightly D-DBA conditions.	[87]
			5	Steam, 1100 °C, 850 s	6.5		
			7		3.5		
			5–12	Steam, 1200 °C, 5 min	1.0 <1		
NiCr/E110	MS	Columnar/Dense	2	Air, 1100 °C, 20 min	>20	-Ni-Cr coatings demonstrate low oxidation resistance compared to pure Cr coatings; -Fast interdiffusion of Ni into the E110 alloy; -Coatings with higher Ni content have lower oxidation resistance and cause fast permeation of hydrogen at 360 °C.	[106]

Table 2. Cont.

Coating/Substrate	Deposition Method	Microstructure	Thickness, μm	Oxidation Conditions	WG, mg/cm^2	Comments	Refs.
Cr_3C_2 - NiCr/Zry-4 Ni-Cr/Zry-4	HVOF	Dense with closed pores	120	Steam, 1200 °C, 1 h	29.8 64.4	-Heterogeneous microstructure of the formed coatings; - Cr_3C_2 -NiCr coating remains intact and shows good oxidation resistance, while Ni-Cr coating is non-protective.	[149]
FeCrAl/Zry-4 (Zirlo) FeCrAl/Mo/Zirlo	CS	Dense	100	Air, 1200 °C, 20 min	–	-Formation of a thick interdiffusion layer of $(\text{Fe,Cr})_2\text{Zr}$ Laves phase with low melting point; -Mo interlayer can act as a diffusion barrier between FeCrAl and zirconium alloy; -Complex structure of the interlayers forms between FeCrAl/Mo and Mo/Zr-alloy interfaces.	[84]
FeCrAl/Mo/Zry-4	dcMS	Dense	6.6/10.6	Steam, 1000–1200 °C, 1 h	–	-The bi-layer coating protects Zry-4 alloy from HT steam oxidation; -Formation of interdiffusion FeCrMo layer between FeCrAl and Mo; -Formation of voids in the FeCrAl coating due to Kirkendall effect.	[177]
Cr/SiC	HiPIMS	Dense	5–15	Steam, 1200 °C, 4 h	0.9	-HiPIMS and HiPIMS+CAPVD coatings are still intact after steam oxidation, but CAPVD coating is partially delaminated;	[34]
	CAPVD	Dense/cracks			1.5	-Cr coatings were fully consumed by oxidation and interdiffusion with the SiC and then the rate was slowed down and controlled by SiO_2 growth;	
	HiPIMS + CAPVD	Dense			1.2	-H generation will be significantly lower than in the case of Zr-based alloy claddings.	
SiC/Zry-4	PECVD	–	1	Autoclave, 350 °C, 20 MPa, 24 h	Weight loss	-Unstable oxide growth; -Volatilization and degradation of coating during autoclave test.	[144]
ZrSi_2 /Zry-4	dcMS	Columnar	3.9	Autoclave, 400 °C, 10.3 MPa, 72 h	Weight loss	-Coating volatilization; -No cracking or spallation are observed after three cycles of water quenching from 700 °C.	[137]
Cr/Zry-4	CAPVD	Dense	10	Steam, 1200 °C, 2000 s	12	-Improved HT oxidation resistance of Cr-coated alloy; -No cracking of the coating after oxidation; -Formation of Cr–Zr interlayer.	[178]
Cr	CS	Dense with some closed pores	50	Steam, 1130–1310 °C for 10–90 min	–	- Parabolic kinetics at 1130 °C changed to quartic at 1230 and 1310 °C, which is attributed in part to the sublimation of Cr species; -Cr–Zr interdiffusion resulted in the formation of brittle ZrCr_2 or $\text{Zr}(\text{Fe,Cr})_2$ intermetallics; -Cr-rich precipitates formed in the depth of Zr alloy after oxidation at 1310 °C.	[179]
Cr_2AlC /Zr702	HiPIMS	Columnar	3.2	Air, 1200 °C, 2 h	2–5	-Cr–Al–C and annealed Cr_2AlC coatings protect Zr alloy in dry or wet air; -Mixed Cr_2O_3 and Al_2O_3 formed during oxidation; -Outward diffusion of Al and Cr and the interdiffusion at the coating/metal interface led to formation of porous (Cr,C) interlayer.	[175]

Table 2. Cont.

Coating/Substrate	Deposition Method	Microstructure	Thickness, μm	Oxidation Conditions	WG, mg/cm^2	Comments	Refs.
$\text{Ti}_2\text{AlC}/\text{TiC}/\text{Zry-4}$	MS	Dense voids-free	5.0/0.5	Steam, 800 °C, 250 min	2.6	- $\text{Ti}_2\text{AlC}/\text{TiC}$ coating demonstrates high oxidation resistance in steam at 800 °C, forming a triple-layered scale $\theta\text{-Al}_2\text{O}_3 + \text{TiO}_2/\theta\text{-Al}_2\text{O}_3/\text{TiO}_2$; -TiC barrier layer mitigates the inward diffusion of Al into the Zry-4 alloy; -Rapid oxidation at 1000 °C resulted in cracking and spallation of the Ti_2AlC coatings.	[157]
				Steam, 1000 °C, 250 min	42.5		
				Steam, 1000 °C, 10 min	0.13		
$\text{Ti}_2\text{AlC}/\text{TiC}/\text{Zirlo}$	hybrid arc/MS	Dense	12.0/1.5	Steam, 1100 °C, 10 min	1.94	- Ti_2AlC coating improves the HT oxidation resistance of ZIRLO alloy during oxidation at up to 1200 °C for 5 min; -Despite TiC barrier layer, the inward diffusion of Al is the main cause of coating failure and rapid consumption for prolonged oxidation times; -Need to prepare thicker coatings and suitable diffusion barriers.	[155]
				Steam, 1200 °C, 5 min	1.17		
				Steam, 1200 °C, 10 min	16.65		
$\text{CrAlN}/\text{Zry-4}$	CAPVD	Dense	5.5	Ar/steam, 1200 °C, up to 1 h	~17.1 (15 min)	-Bilayer structure of the formed oxides: an outer Cr-rich mixed $\text{Cr}_2\text{O}_3\text{-Al}_2\text{O}_3$ layer and an inner Al-rich mixed ($\text{Al}_2\text{O}_3\text{-Cr}_2\text{O}_3$ in CrAlN and $\text{Al}_2\text{O}_3\text{-Cr}_2\text{O}_3\text{-SiO}_2$ in CrAlSiN) layer; - Phase transition $\text{c-AlN} \rightarrow \text{h-AlN}$ and $\text{CrN} \rightarrow \text{Cr}_2\text{N}$) and subsequent substrate nitriding;	[176]
$\text{CrAlSiN}/\text{Zry-4}$			5.8		~14.8 (15 min)	-Inferior oxidation resistance of the CrAlSiN compared to the CrAlN coating due to cracking in HT steam caused by the formation of nanosized Si_3N_4 grains.	
$\text{AlCrMoNbZr}/\text{N36}$ (Zr-1Sn-1Nb-0.3Fe)	MS	Dense	3	Autoclave, 360 °C, 18.6 MPa, 30 days	0.09	-AlCrMoNbZr HEA improves the oxidation resistance of N36 alloy by 3 times; -Multiphase oxide ($\text{Nb}_2\text{Zr}_6\text{O}_{17}$, ZrO_2 and Cr_2O_3) formed on the coating surface.	[115]

Note: WG—weight gain, PVD—physical vapor deposition, PE-CVD—plasma enhanced chemical vapor deposition, CS—cold spraying, MS—magnetron sputtering, CAPVD—cathodic arc physical vapor deposition, HiPIMS—high power impulse magnetron sputtering, dcMS—direct current magnetron sputtering, HVOF—high velocity oxygen fuel.

4.2. Interdiffusion and Eutectics under B-DBA Conditions

The interdiffusion of coating elements has a complex negative effect related to the rapid consumption of the coating and the formation of anisotropic structures inside the Zr alloys, as a result of the formation and subsequent crystallization of liquid eutectic phases. These processes accelerate with increasing temperature, so that the behavior of protective materials under B-DBA conditions is highly important for the development of ATF Zr claddings.

Brachet et al. investigated the behavior of Cr-coated M5 alloy under steam oxidation at 1400–1450 °C for 100 s, followed by water quenching [166]. It was found that the rapid mutual Cr–Zr diffusion during heating is accompanied by the formation of Cr–Zr eutectics at 1305–1325 °C, which are gradually enriched with zirconium along with the growth of the outer ZrO_2 / α -Zr(O) oxide layers at the isothermal oxidation period. After water quenching, a dendritic substructure of the Cr-depleted prior- β_{Zr} and Cr-enriched interdendritic zones form inside the alloy, and a “crocodile skin”-like morphology of the coated alloy was observed (Figure 14). Krejci et al. observed similar microstructures of Cr-coated E110 alloy after HT steam oxidation at 1400 °C for 2 min [134]. A higher Cr content was found in the region of the prior β_{Zr} phase (with lower oxygen content).

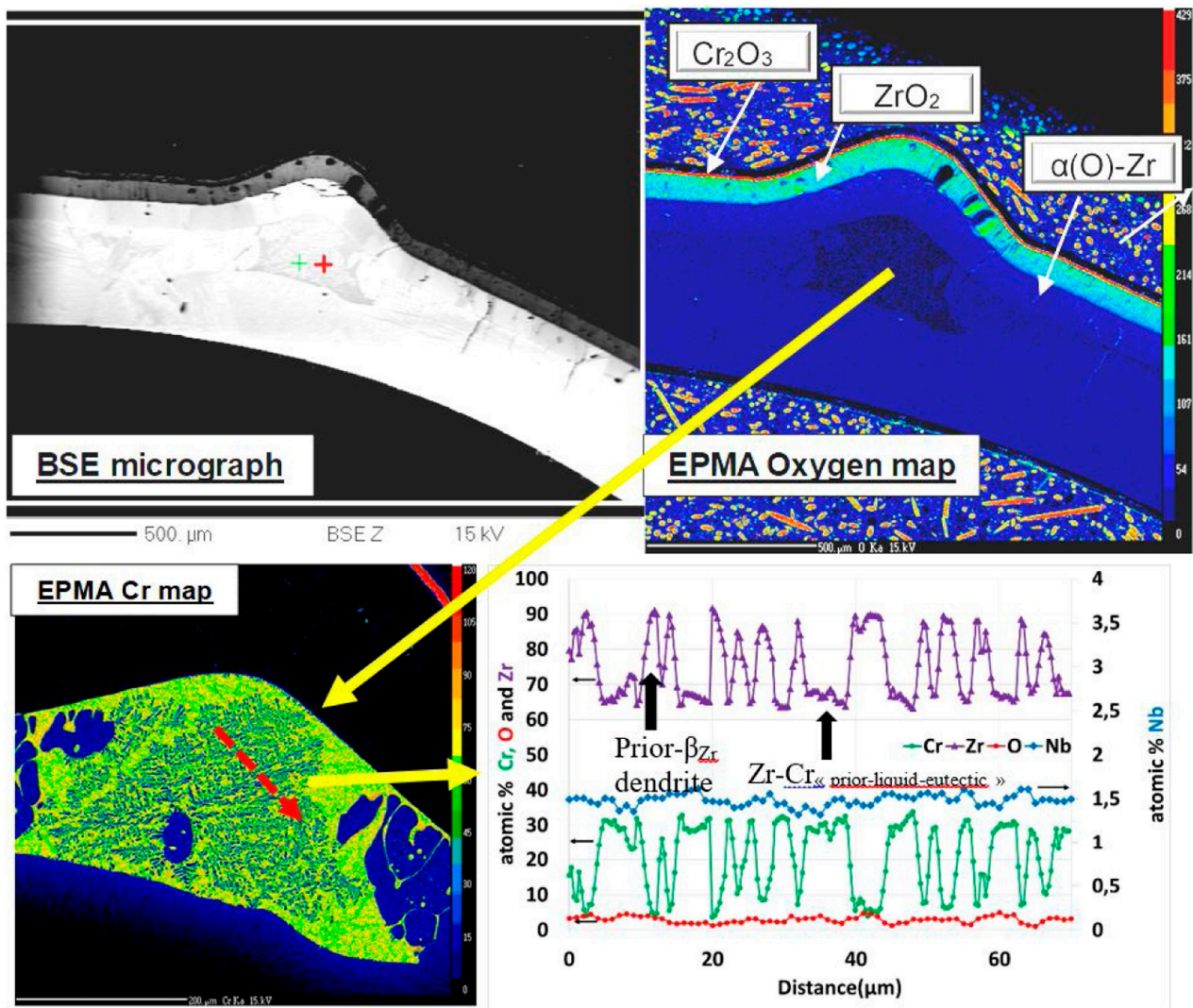


Figure 14. Microstructure of 12–15 μm thick Cr-coated M5 Framatome cladding segment after steam oxidation at 1400 °C for 100 s, followed by water quenching. Reproduced from [166] with permission by Elsevier.

Interdiffusion also shows a negative effect on FeCrAl-coated Zr alloys [180]. In this case, the fast diffusion of Fe and Cr resulted in the formation of brittle intermetallic compounds such as Fe_2Zr , FeZr_2 , FeZr_3 and $\text{Zr}(\text{Cr,Fe})_2$, as well as in a low melting-point of Zr-Fe or Zr-Fe-Cr eutectic phases [81,85,181]. Thus, the eutectic phases and the mismatch of CTE between Zr alloy and intermetallics can cause the formation of a non-protective scale on the oxides and the generation of micro-cracks. Wang et al. demonstrated the oxidation behavior of FeCrAl coating, with a ZrO_2 barrier layer formed by plasma electrolytic oxidation (PEO) on a Zry-4 alloy surface. It was found that a 10–15 μm -thick ZrO_2 layer eliminates the diffusion of Fe and Cr to the alloy in steam at 1000 °C [182]. Nevertheless, more detailed studies of oxidation behavior at higher temperatures are needed. Han et al. demonstrated good barrier properties of a 10.6 μm Mo interlayer between a 6.6 μm FeCrAl coating and a Zry-4 alloy under steam oxidation up to 1200 °C [177]. Despite the better oxidation resistance of FeCrAl/Mo coatings, a strong interdiffusion between Mo and FeCrAl layers at 1200 °C resulted in the formation of a FeCrMo interlayer, accompanied by generation of Kirkendall voids in the FeCrAl coating.

Krejci et al. investigated a stoichiometric CrN interlayer deposited by magnetron sputtering as the barrier against Cr-Zr interdiffusion at HT steam oxidation [183]. It was found that a thin ZrN layer formed beneath the coating due to the inward diffusion of nitrogen generated from the decomposition of CrN to Cr_2N phase. The 13 μm -thick CrN layer inhibited the diffusion of Cr to Zr alloy, and demonstrated high oxidation resistance at temperatures above the Cr-Zr eutectic (1350 °C) for only a short period (Figure 15). Tang et al. showed that a 500 nm TiC interlayer mitigates the rapid diffusion of Al from Ti_2AlC coating into the Zry-4 alloy, which resulted in a prolonged oxidation resistance of Ti_2AlC /TiC coating under 800 °C steam [157]. However, both Ti_2AlC and Ti_2AlC /TiC coatings demonstrated low oxidation performance at temperatures higher than 1000 °C.

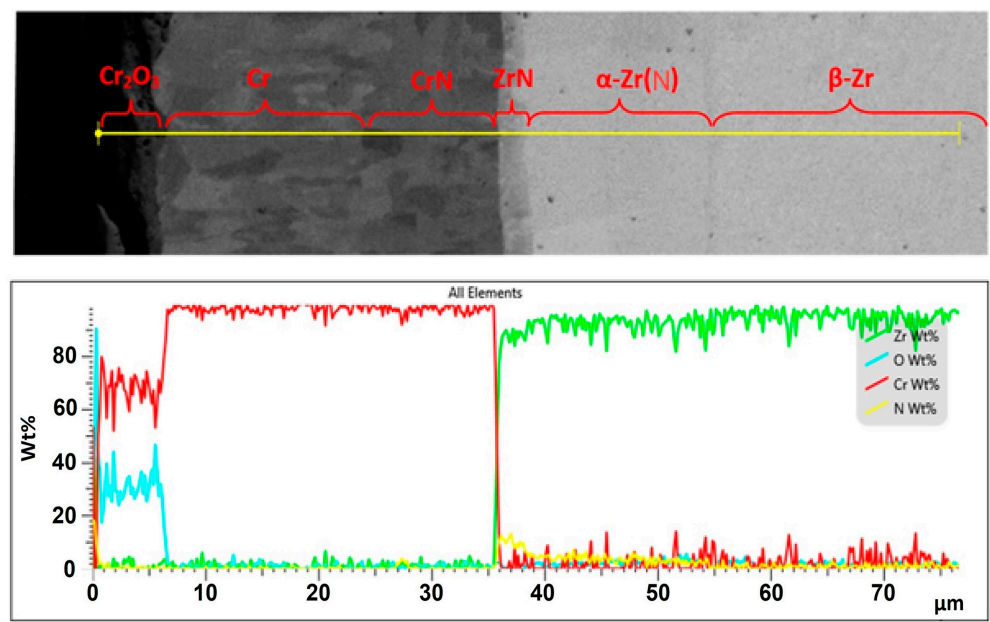


Figure 15. Microstructure of Cr/CrN-coated Zr-1%Nb alloy after HT oxidation in steam at 1365 °C for 2 min: SEM image and corresponding EDS line scan. Reproduced from [183] with permission by Elsevier.

The abovementioned studies confirm the promising approach of barrier layers for suppressing interdiffusion between protective coating and zirconium alloys under B-DBA conditions. However, there are many factors that should be considered when choosing an intermediate layer, such as possible formation of eutectic phases, low melting point, high diffusion coefficient in Zr, large difference in thermal expansion coefficients, possible

phase transitions, etc. Table 3 shows some of the possible interlayers between Cr coating and Zr alloys, and indicates their most important properties in terms of barrier coating for ATF. Diffusion coefficients in zirconium strongly depend on the presence of impurities, and their reported values differ significantly in the published works. Therefore, only relative diffusion characteristics (coefficients) are given in Table 3 for comparison. Considering interlayer materials, their thermal neutron cross-sections should also be discussed in view of possible changes in neutron economy [184]. The multiplication factor, reactivity, neutron spectra and reactivity coefficient will change even with very thin coatings [185]. It can limit interlayer thickness to minimize neutron losses.

Table 3. Comparison of properties of possible barrier layers between Cr-based coatings and zirconium alloys. Zirconium and chromium are presented for comparison.

Interlayer	Possible Eutectics	T_m , °C	Diffusion Coefficient in β -Zr	Solubility in β -Zr at 1300 °C	CTE at RT, 10^{-6} K^{-1}	λ , W/m/K	Phase Transitions	Mechanical Behavior
Zr	—	1855	—	—	7.2 (hcp) 9.6 (bcc)	22	$\alpha_{\text{hcp}} \rightarrow \beta_{\text{bcc}}$ at 862 °C	Ductile
Cr	1330 °C (Cr-Zr)	1907	High	<8 at. %	6.5	93.7	no	Ductile/Brittle
Mo	1550 °C (Mo-Zr) 1820 °C	2623	Low	<30 at. %	5.5	138	no	Ductile
Ta	(Ta-Zr) 1760 °C (Ta-Cr)	3017	Low	~15 at. %	6.5	57.5	Only for metastable $\beta \rightarrow \alpha$ at 750–775 °C	Ductile
Nb	1668 °C (Nb-Cr)	2477	High	100 at. %	7.1	53.7	no	Ductile
Re	1600 °C (Re-Zr)	3186	Unknown	~10 at. %	6.1–6.6	39.6	no	Ductile
CrN (Cr ₂ N)	—	1770	N diffusion due to CrN \rightarrow Cr ₂ N	—	9.0–9.4	2–5 (CrN); 12 (Cr ₂ N)	CrN \rightarrow Cr ₂ N at HT	Brittle
Cr ₂ O ₃	—	2330	—	—	7.1	12	no	Brittle
ZrO ₂	—	2715	—	—	7 (m-ZrO ₂) 12 (t-ZrO ₂)	1.7 (m-ZrO ₂)	t \rightarrow m-ZrO ₂ (high volume expansion)	Brittle
ZrC	—	3532	—	—	6.7	20.5	no	Brittle
3C-SiC	1370 °C (Zr-Si)	2830	—	—	4.3	270	no	Brittle

Note: T_m —melting point, CTE—coefficient of thermal expansion, RT—room temperature, λ —thermal conductivity.

Molybdenum is considered one of the most promising interlayers since it shows good barrier properties, a CTE similar to Cr, high thermal conductivity, a high melting point and an acceptable neutron cross-section (2.5 barn). Moreover, the potential eutectic phase of Mo-Zr has a higher melting temperature (1550 °C) compared to Cr-Zr (1330 °C). Nevertheless, coupled effects of the Cr-Mo-Zr system (eutectics) should be considered. Recently presented results obtained at CEA showed some interesting and positive observations on Cr/Mo-coated zirconium alloy (not published yet, but please see Michau et al., Numat-2020). It has been shown that a Mo/Cr coating demonstrates good oxidation resistance in steam up to 1400 °C for 100 s. The Mo interlayer can delay the Cr-Zr eutectic reaction and reduce Cr consumption by interface reactions. However, detailed studies on coating architecture, adhesion, irradiation behavior and oxidation resistance under normal operation conditions are still required.

A tantalum interlayer can also be promising for enhancing the performance of Cr-coated alloys under B-DBA conditions, since it has a low diffusion coefficient and solubility limit in β -Zr phase, as well as CTE close to Cr. In addition, melting temperatures of possible eutectic phases are higher than that of the Cr-Mo-Zr system. The thermal conductivity of Ta is lower than that of chromium, but higher than that of zirconium. However, the high thermal neutron cross-section of Ta (20.6 barn) can strongly limit the thickness of the Ta layer in the protective coating, thus saving of neutron economy and decrease neutron losses.

Unfortunately, there are no studies on Ta diffusion in zirconium at high temperatures and HT oxidation of Cr/Ta/Zr or Ta/Zr systems. Despite a lack of studies, a Ta interlayer could potentially be effective and should be studied in future research.

Niobium is already used as an alloying element in Zr-Nb alloys and has a high melting point in the Nb-Cr and Nb-Zr systems, and a CTE close to that of zirconium. Nb has a low diffusion coefficient in α -Zr phase [181] and a neutron cross-section of 1.2 barn. However, high interdiffusion between Nb and Zr is expected due to the unlimited solubility of Nb in the β -Zr phase at temperatures above 970 °C, which is also supported by high values of diffusion coefficients measured between Nb and Zr in the β phase, including Nb in Zr-1Nb alloy [186,187].

Rhenium is a transition metal with a very high melting point (3186 °C), which forms a eutectic phase with Zr at high temperature (1600 °C) and has a low solubility limit in the β -Zr phase. The CTE of Re is close to that of Cr, while thermal conductivity is between Cr and Zr. However, Re is one of the rarest elements and has a very high neutron cross-section (89.7 barn); therefore, this material is considered economically unfavorable in terms of supply risk, environmental implications and vulnerability to supply restrictions [188].

Ceramic coatings such as CrN (Cr₂N), Cr₂O₃, ZrO₂, ZrC and SiC are also good candidates for barrier interlayers due to their high temperature stability, high melting point and low diffusion rate compared to metallic coatings. CrN coatings demonstrate barrier properties at temperatures above 1350 °C; however, only for thick interlayers, as described above. The decomposition of CrN \rightarrow Cr₂N results in the formation of a zirconium nitride layer, which also plays an important role in reducing the diffusion of Cr into Zr alloy. The CTE of CrN is similar to that of the β -Zr phase. Nevertheless, a very low thermal conductivity of chromium nitrides coatings and the phase transformation (fcc to hcp) accompanied by volume reduction should be taken into account when selecting thick CrN layers as interlayer coatings. Zirconium carbide can be potentially used since it has an intermediate CTE and thermal conductivity comparable to that of Zr. Silicon carbide, and with a cubic (3C) structure that is well-studied since it is one of the most prospective materials for ATF claddings [189–191]. However, its significantly lower CTE compared to Cr and Zr, as well as possible reactions with Zr, limit its application as a barrier interlayer coating for B-DBA conditions. The literature data showed good barrier properties of ZrO₂; for example, in the case of FeCrAl coatings [182]. When choosing such a type of interlayer, it is necessary to take into account its very low thermal conductivity and possible phase transformation (t -ZrO₂ \rightarrow m -ZrO₂) with high volume expansion. Therefore, detailed studies of the barrier properties of ZrO₂ and its behavior under high-temperature oxidation conditions are required. In addition to the other coatings, Cr₂O₃ can also be a promising material for a barrier interlayer, as it has a suitable CTE and good oxidation resistance.

Although the barrier properties of ceramic coatings are more advantageous, they are brittle, and small changes in CTE with temperature can lead to the formation of microcracks and coating failures at the coating/alloy interface. Multilayer ceramic coatings can be more resistant to coating interruption if they are composed of alternating brittle and elastic layers. Musil demonstrated [192,193] two approaches to prevent cracking of brittle coatings. The first way comprises the deposition of a highly elastic over-layer on top of the brittle layer, while the second is the reduction in the macrostress of multilayered structures [194]. Therefore, a multilayer approach with an appropriate design can be an effective way to reduce the CTE difference and improve the cracking resistance of protective ceramic coatings. Moreover, multilayers can be used as a barrier layer to prevent Cr–Zr interdiffusion, while a top chromium coating with high thickness can act as the main protective layer.

Sidelev et al. demonstrated the barrier properties of multilayer CrN/Cr (250/250 nm) coatings against Cr-Zr inter-diffusion during heating up to 1400 °C (Figure 16) [195]. It was found that the diffusion limitation was attributed not only to CrN layers but also to a ZrN layer formed beneath the multilayers due to the decomposition of chromium nitrides at high temperatures (650–900 °C). Furthermore, a better oxidation performance

of CrN/Cr coatings compared to metallic Cr coating was shown during air oxidation at 1100 °C for 10–40 min. No coating cracking or local oxidation were observed for multilayer coatings with layer steps of 250/250 and 500/500 nm, while multilayer 50/50 nm coating demonstrated accelerated oxidation after a 30 min test.

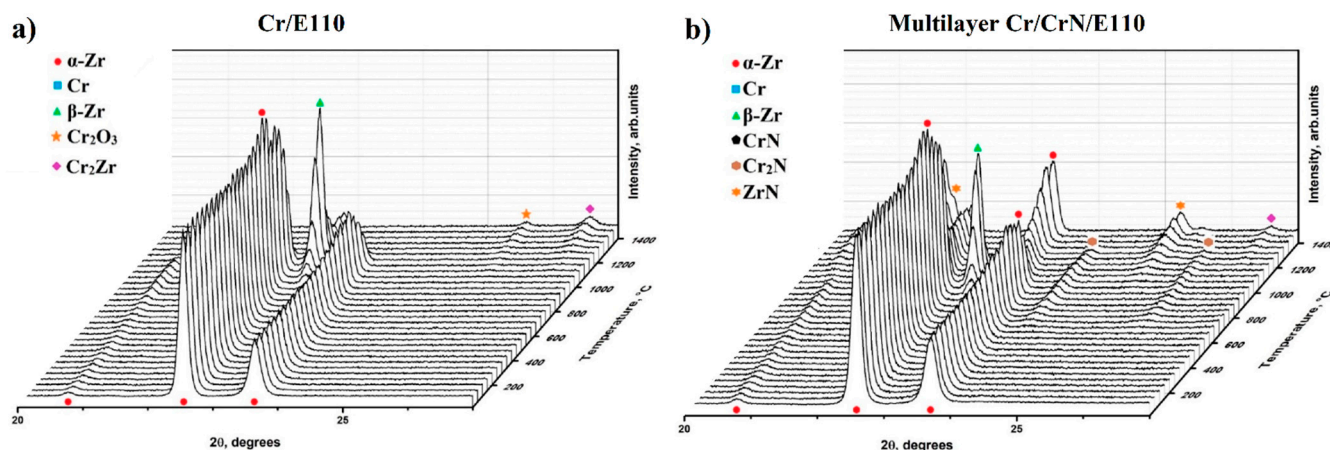


Figure 16. In situ XRD patterns of an E110 alloy with single-layer Cr (a) and multilayer Cr/CrN (b) (layer step-250 nm) coatings under linear heating in the temperature range of 25–1400 °C. Replotted from [195].

5. Concluding Remarks

In summary, various coatings for ATF zirconium alloy claddings are considered. The protective properties of coatings under conditions simulating normal and accidental operation of LWRs have been analyzed. Positive and negative aspects of metallic and non-metallic coatings for ATF applications were considered. Several ceramic coatings, e.g., chromium nitrides and carbides, show good results in high-temperature oxidation, but their brittle nature and difference of thermal expansion coefficients with Zr alloys largely limit their use as a single-layer protective coating on outer Zr cladding surfaces. Promising radiation-resistant coatings based on MAX-phases have good protective properties up to 1000 °C; however, they show poor oxidation resistance at higher temperatures or should have high thickness. High-entropy alloys are promising as cladding materials, but display poor corrosion resistance in pressurized water due to the formation of complex heterophase composition of the oxides, some of which may dissolve in water under normal operation conditions. Chromium oxide (Cr_2O_3) is the most stable oxide phase in water and steam, which is why a dense protective chromia scale is the most preferable option for ATF applications.

Our analysis of the literature data indicates promising uses for Cr-based coatings for normal, DBA and B-DBA conditions. The application of various industrial deposition technologies to deposit Cr coatings onto Zr-based alloys has been shown. Physical vapor deposition, primarily multi-cathode magnetron sputtering or HiPIMS have great prospects for the development of coating technology for ATF Zr-based claddings. The optimization of deposition parameters to obtain dense columnar-free Cr coatings with high adhesion and mechanical characteristics has been carried out. The technology of magnetron sputtering on full-length Zr-based fuel claddings was developed by CEA. In addition, fuel Zr claddings with Cr-based coatings are currently undergoing in-pile testing; for example, in the Russian research reactor MIR. Nevertheless, an important and relevant issue remains related to the behavior of protective coatings under B-DBA conditions, where strong mutual diffusion between the coating and the zirconium cladding can be expected. This effect is evident in most metallic coatings (including chromium), as well as MAX-phase coatings, even at temperatures below DBA. Accordingly, an important future step is the development of barrier layers that can limit interdiffusion and also meet the basic requirements for reactor materials. This review showed the results achieved for protective coatings with barrier

layers, and suggested possible interlayers and designs of multilayer structures that might be considered in the future. Therefore, the selection of appropriate diffusion barrier layers, such as Mo, Ta, ZrO₂, Cr₂O₃, ZrC, etc., is still open for investigation. The thickness of the barrier layer and the protective coating should be determined in view of neutron economy, oxidation resistance and barrier efficiency. For the most promising systems, out-of-pile and in-pile testing of protective coatings with barrier layers are necessary. In the case of ceramic barrier layers, cracking resistance must be clearly studied.

Author Contributions: Conceptualization, E.K. and D.S.; validation, E.K., D.S., and A.L.; formal analysis, A.L.; investigation, D.S. and V.G.; resources, A.L.; data curation, D.S.; writing—original draft preparation, E.K. and B.A.; writing—review and editing, D.S., V.G., and M.K.; visualization, E.K.; supervision, E.K.; project administration, E.K.; funding acquisition, E.K. and D.S. All authors have read and agreed to the published version of the manuscript.

Funding: The reported study was supported by the Russian Science Foundation, Grant No. 19-79-10116.

Institutional Review Board Statement: Not applicable.

Informed Consent Statement: Not applicable.

Data Availability Statement: This is a review article, and the entire data is presented within the article. The data presented in Figure 16 are available on request from the corresponding author.

Acknowledgments: The research is conducted within the framework of National Research Tomsk Polytechnic University Competitiveness Enhancement Program.

Conflicts of Interest: The authors declare no conflict of interest.

Abbreviations

Accident Tolerant Fuel (ATF), Beyond Design Basis Accident (B-DBA), Boiling Water Reactor (BWR), Cathodic Arc Physical Vapor Deposition (CAPVD), Coefficient of Thermal Expansion (CTE), Cold Spraying (CS), Design Basis Accident (DBA), Direct Liquid Injection – Metalorganic Chemical Vapor Deposition (DLI-MOCVD), Equivalent Cladding Reacted (ECR), High Entropy Alloy (HEA), High Power Impulse Magnetron Sputtering (HiPIMS), High Temperature (HT), High Velocity Oxygen Fuel (HVOF), Light-Water Reactor (LWR), Loss of Coolant Accident (LOCA), Magnetron Sputtering (MS), Plasma Enhanced Chemical Vapor Deposition (PE-CVD), Pressurized Water Reactor (PWR), Physical Vapor Deposition (PVD), Reaktor Bolshoy Moschnosti Kanalnyy (RBMK), Research and Development (R&D), Silicon Carbide (SiC), Water-Water Energetic Reactor (VVER), Weight Gain (WG), Zirconium Low Oxidation (ZIRLO).

References

1. Azhazha, V.; Borts, B.; Butenko, I.; Voevodin, V.; V'yugov, P.; Gritsina, V.; Krasnorutskij, V.; Lavrinenko, S.; Levenets, V.; Neklyudov, I. *Zirconium-Niobium Alloys for NPP*; Splav Tsirkonij-Niobij Dlya AehS: Alushta, Ukraine, 2012.
2. Zieliński, A.; Sobieszczyk, S. Hydrogen-enhanced degradation and oxide effects in zirconium alloys for nuclear applications. *Int. J. Hydrog. Energy* **2011**, *36*, 8619–8629. [\[CrossRef\]](#)
3. Charit, I. Accident tolerant nuclear fuels and cladding materials. *JOM* **2018**, *70*, 173–175. [\[CrossRef\]](#)
4. Motta, A.T.; Capolungo, L.; Chen, L.Q.; Cinbiz, M.N.; Daymond, M.R.; Koss, D.A.; Lacroix, E.; Pastore, G.; Simon, P.-C.A.; Tonks, M.R.; et al. Hydrogen in zirconium alloys: A review. *J. Nucl. Mater.* **2019**, *518*, 440–460. [\[CrossRef\]](#)
5. Baba, M. Fukushima accident: What happened? *Radiat. Meas.* **2013**, *55*, 17–21. [\[CrossRef\]](#)
6. National Research Council. Lessons learned from the Fukushima nuclear accident for improving safety of US nuclear plants. *Natl. Acad. Sci.* **2014**, *394*. [\[CrossRef\]](#)
7. Shebaldov, P.; Peregud, M.M.; Nikulina, A.; Bibilashvili, Y.K.; Lositski, A.; Kuz'menko, N.; Belov, V.; Novoselov, A. E110 alloy cladding tube properties and their interrelation with alloy structure-phase condition and impurity content. In Proceedings of the Zirconium in the Nuclear Industry: Twelfth International Symposium, West Conshohocken, PA, USA, 15–18 June 1998.
8. Pellegrini, M.; Herranz, L.; Sonnenkalb, M.; Lind, T.; Maruyama, Y.; Gauntt, R.; Bixler, N.; Morreale, A.; Dolganov, K.; Sevón, T. Main findings, remaining uncertainties and lessons learned from the OECD/NEA BSAF project. *Nucl. Technol.* **2020**, *206*, 1449–1463. [\[CrossRef\]](#)

9. Zinkle, S.J.; Terrani, K.A.; Gehin, J.C.; Ott, L.J.; Snead, L.L. Accident tolerant fuels for LWRs: A perspective. *J. Nucl. Mater.* **2014**, *448*, 374–379. [[CrossRef](#)]
10. Terrani, K.A.; Zinkle, S.J.; Snead, L.L. Advanced oxidation-resistant iron-based alloys for LWR fuel cladding. *J. Nucl. Mater.* **2014**, *448*, 420–435. [[CrossRef](#)]
11. Karoutas, Z.; Brown, J.; Atwood, A.; Hallstadius, L.; Lahoda, E.; Ray, S.; Bradfute, J. The maturing of nuclear fuel: Past to Accident Tolerant Fuel. *Prog. Nucl. Energy* **2018**, *102*, 68–78. [[CrossRef](#)]
12. Carmack, J.; Goldner, F.; Bragg-Sitton, S.M.; Snead, L.L. *Overview of the US DOE Accident Tolerant Fuel Development Program*; Idaho National Laboratory (INL): Idaho, ID, USA, 2013.
13. Kim, D.; Lee, H.-G.; Park, J.Y.; Kim, W.-J. Fabrication and measurement of hoop strength of SiC triplex tube for nuclear fuel cladding applications. *J. Nucl. Mater.* **2015**, *458*, 29–36. [[CrossRef](#)]
14. Katoh, Y.; Snead, L.L.; Henager Jr, C.H.; Nozawa, T.; Hinoki, T.; Iveković, A.; Novak, S.; De Vicente, S.G. Current status and recent research achievements in SiC/SiC composites. *J. Nucl. Mater.* **2014**, *455*, 387–397. [[CrossRef](#)]
15. Zhou, X.; Wang, H.; Zhao, S. Progress of SiCf/SiC composites for nuclear application. *Adv. Ceram.* **2016**, *37*, 151–167.
16. Qiu, B.; Wang, J.; Deng, Y.; Wang, M.; Wu, Y.; Qiu, S. A review on thermohydraulic and mechanical-physical properties of SiC, FeCrAl and Ti3SiC2 for ATF cladding. *Nucl. Eng. Technol.* **2020**, *52*, 1–13. [[CrossRef](#)]
17. Liu, J.; Zhang, X.; Yun, D. A complete review and a prospect on the candidate materials for accident-tolerant fuel claddings. *Mater. Rev.* **2018**, *32*, 1757–1778.
18. Bragg-Sitton, S.M.; Todosow, M.; Montgomery, R.; Stanek, C.R.; Montgomery, R.; Carmack, W.J. Metrics for the technical performance evaluation of light water reactor accident-tolerant fuel. *Nucl. Technol.* **2016**, *195*, 111–123. [[CrossRef](#)]
19. Chen, H.; Wang, X.; Zhang, R. Application and development progress of Cr-based surface coatings in nuclear fuel element: I. selection, preparation, and characteristics of coating materials. *Coatings* **2020**, *10*, 808. [[CrossRef](#)]
20. Chen, H.; Wang, X.; Zhang, R. Application and Development Progress of Cr-Based Surface Coating in Nuclear Fuel Elements: II. Current Status and Shortcomings of Performance Studies. *Coatings* **2020**, *10*, 835. [[CrossRef](#)]
21. Terrani, K.A. Accident tolerant fuel cladding development: Promise, status, and challenges. *J. Nucl. Mater.* **2018**, *501*, 13–30. [[CrossRef](#)]
22. Cheng, B. Fuel behavior in severe accidents and Mo-alloy based cladding designs to improve accident tolerance. *Atw. Int. Z. Fuer Kernenerg.* **2013**, *59*, 158–160.
23. Nelson, A.; Sooby, E.; Kim, Y.-J.; Cheng, B.; Maloy, S. High temperature oxidation of molybdenum in water vapor environments. *J. Nucl. Mater.* **2014**, *448*, 441–447. [[CrossRef](#)]
24. Cheng, B.; Chou, P.; Kim, Y.-J. Evaluations of Mo-alloy for light water reactor fuel cladding to enhance accident tolerance. *EPJ Nucl. Sci. Technol.* **2016**, *2*, 5. [[CrossRef](#)]
25. Cheng, B.; Chou, P.; Kim, Y.-J. *Development of Mo-Based Accident Tolerant LWR Fuel Cladding*; International Atomic Energy Agency: Vienna, Austria, 2016.
26. Karpyuk, L.; Savchenko, A.; Leont'eva-Smirnova, M.; Kulakov, G.; Konovalov, Y.V. Steel Cladding for VVER Fuel Pins in the Context of Accident-Tolerant Fuel: Prospects. *At. Energy* **2020**, *128*, 218–222. [[CrossRef](#)]
27. Guanghai, B.; Zhilin, C.; Yanwei, Z.; Erwei, L.; Jiaxiang, X.; Weiwei, Y.; Rongshan, W.; Rui, L.; Tong, L. Research progress of coating on zirconium alloy for nuclear fuel cladding. *Rare Met. Mater. Eng.* **2017**, *46*, 2035–2040.
28. Maier, B.; Yeom, H.; Johnson, G.; Dabney, T.; Walters, J.; Romero, J.; Shah, H.; Xu, P.; Sridharan, K. Development of cold spray coatings for accident-tolerant fuel cladding in light water reactors. *JOM* **2018**, *70*, 198–202. [[CrossRef](#)]
29. Lustman, B. Zirconium technology—twenty years of evolution. In *Zirconium in the Nuclear Industry*; ASTM International: West Conshohocken, PA, USA, 1979.
30. Baczynski, J. High Temperature Steam Oxidation of Titanium-Coated Zircaloy-2 and Titanium-Zirconium Alloys. Master's Thesis, University of Illinois at Urbana-Champaign, Urbana, IL, USA, 2014.
31. Kim, H.-G.; Kim, I.-H.; Jung, Y.-I.; Park, D.-J.; Yang, J.-H.; Koo, Y.-H. Development of surface modified Zr cladding by coating technology for ATF. *Proc. Top Fuel* **2016**, 1157–1163.
32. Sagiroun, M.I.; Xinrong, C. Zirconium-Based Cladding Coating Technique for Oxidation, Corrosion and Embrittlement Reduction at High-Temperature: An Overview. *IOP Conf. Ser. Mater. Sci. Eng.* **2019**, *649*, 012008. [[CrossRef](#)]
33. Barrett, F.; Huang, X.; Guzonas, D. Characterization of TiO₂-doped yttria-stabilized zirconia (YSZ) for supercritical water-cooled reactor insulator application. *J. Therm. Spray Technol.* **2013**, *22*, 734–743. [[CrossRef](#)]
34. Kane, K.A.; Stack, P.; Mouche, P.A.; Pillai, R.R.; Pint, B.A. Steam oxidation of chromium corrosion barrier coatings for sic-based accident tolerant fuel cladding. *J. Nucl. Mater.* **2021**, *543*, 152561. [[CrossRef](#)]
35. Chen, Q.; Liu, C.; Zhang, R.; Yang, H.; Wei, T.; Wang, Y.; Li, Z.; He, L.; Wang, J.; Wang, L. Microstructure and high-temperature steam oxidation properties of thick Cr coatings prepared by magnetron sputtering for accident tolerant fuel claddings: The role of bias in the deposition process. *Corros. Sci.* **2020**, *165*, 108378. [[CrossRef](#)]
36. Rickover, H.G.; Geiger, L.D.; Lustman, B. *History of the Development of Zirconium Alloys for Use in Nuclear Reactors*; Energy Research and Development Administration: Washington, DC, USA, 1975.
37. Gadiyar, H. Corrosion of zirconium base alloys—an overview. In *Proceedings of Symposium on Zirconium Alloys for Reactor Components*; Bhabha Atomic Research Centre: Bombay, India, 1992.

38. Kass, S. The development of the zircaloys. In *Corrosion of Zirconium Alloys*; ASTM International: West Conshohocken, PA, USA, 1964.
39. Motta, A.T.; Couet, A.; Comstock, R.J. Corrosion of zirconium alloys used for nuclear fuel cladding. *Annu. Rev. Mater. Res.* **2015**, *45*, 311–343. [\[CrossRef\]](#)
40. Cox, B. Some thoughts on the mechanisms of in-reactor corrosion of zirconium alloys. *J. Nucl. Mater.* **2005**, *336*, 331–368. [\[CrossRef\]](#)
41. Alam, T.; Khan, M.K.; Pathak, M.; Ravi, K.; Singh, R.; Gupta, S. A review on the clad failure studies. *Nucl. Eng. Des.* **2011**, *241*, 3658–3677. [\[CrossRef\]](#)
42. Moorthy, K.B. *Current trends in the Use of Zirconium Alloys*; National Metallurgical Laboratory: Jamshedpur, India, 1969.
43. Shimada, S.; Cheng, B.; Lutz, D.; Kubota, O.; Ichikawa, N.; Ibe, H. In-core tests of effects of BWR water chemistry impurities on zircaloy corrosion. In *Zirconium in the Nuclear Industry: Fourteenth International Symposium*; ASTM International: West Conshohocken, PA, USA, 2005.
44. Krishnan, R.; Asundi, M. Zirconium alloys in nuclear technology. *Proc. Indian Acad. Sci. Sect. C Eng. Sci.* **1981**, *4*, 41–56.
45. *The Fukushima Daiichi Nuclear Power Plant Accident*; OECD: Paris, France, 2013.
46. Nikulina, A. Zirconium alloys in nuclear power engineering. *Met. Sci. Heat Treat.* **2004**, *46*, 458–462. [\[CrossRef\]](#)
47. Nikulina, A.V.; Markelov, V.; Perehud, M.; Bibilashvili, Y.K.; Kotrekhov, V.; Lositsky, A.; Kuzmenko, N.; Shevnin, Y.P.; Shamardin, V.; Kobylansky, G. Zirconium alloy E635 as a material for fuel rod cladding and other components of VVER and RBMK cores. In *Zirconium in the Nuclear Industry: Eleventh International Symposium*; ASTM International: West Conshohocken, PA, USA, 1996.
48. Markelov, V.; Novikov, V.; Nikulina, A.; Konkov, V.; Sablin, M.; Novoselov, A.; Kobylansky, J. Application of E635 alloy as structural components of WWER-1000 fuel assemblies. In Proceedings of the International Conference on WWER fuel Performance, Modelling and Experimental Support, Albena Bulgaria, 19–23 September 2005.
49. Hózer, Z.; Győri, C.; Matus, L.; Horváth, M. Ductile-to-brittle transition of oxidised Zircaloy-4 and E110 claddings. *J. Nucl. Mater.* **2008**, *373*, 415–423. [\[CrossRef\]](#)
50. Novikov, V.; Nesterov, B.; Troyanov, V.; Izhutov, A.; Burukin, A.; Shahmut, E. Out of reactor investigation corrosive characteristics cladding of new Zirconium alloys as applied to conditions reactor-plant WWER-1200 (AES-2006) and program irradiation tests of this alloys. In Proceedings of the International Conference on WWER Fuel Performance, Modelling and Experimental Support, Albena, Bulgaria, 17–24 September 2011.
51. Novikov, V.; Markelov, V.; Gusev, A.; Malgin, A.; Kabanov, A.; Pimenov, Y. Some results on the properties in-vestigations of zirconium alloys for WWER-1000 fuel cladding. In Proceedings of the International Conference on WWER Fuel Performance, Modelling and Experimental Support, Albena, Bulgaria, 17–24 September 2011.
52. Foster, J.P.; Yueh, H.K.; Comstock, R.J. ZIRLO TM cladding improvement. *J. Astm Int.* **2008**, *5*, 1–13. [\[CrossRef\]](#)
53. Le Saux, M.; Vandenberghe, V.; Crébier, P.; Brachet, J.; Gilbon, D.; Mardon, J.; Jacques, P.; Cabrera, A. Influence of steam pressure on the high temperature oxidation and post-cooling mechanical properties of Zircaloy-4 and M5 cladding (LOCA conditions). In *Zirconium in the Nuclear Industry: 17th Volume*; ASTM International: West Conshohocken, PA, USA, 2015.
54. Brachet, J.-C.; Portier, L.; Forgeron, T.; Hivroz, J.; Hamon, D.; Guilbert, T.; Bredel, T.; Yvon, P.; Mardon, J.-P.; Jacques, P. Influence of hydrogen content on the α/β phase transformation temperatures and on the thermal-mechanical behavior of Zy-4, M4 (ZrSnFeV), and M5TM(ZrNbO) alloys during the first phase of LOCA transient. In *Zirconium in the Nuclear Industry: Thirteenth International Symposium*; ASTM International: West Conshohocken, PA, USA, 2002.
55. Wakamatsu, A.; Nunokawa, K.; Nakano, M.; Hamasaki, M.; Uno, Y.; Kawagoe, T. Development of advanced fuel and core for high reliability and high performance. *Mitsubishi. Juko Giho.* **2006**, *43*, 20–24.
56. Malgin, A.G.; Markelov, V.A.; Novikov, V.V.; Shelepov, I.A.; Donnikov, V.E.; Latunin, V.I.; Krejci, J. Research of high-temperature oxidation behavior of E110 opt and E110M sponge based zirconium alloys. *Proc. Top Fuel* **2018**, *239*, 1–10.
57. Pawel, R.E.; Cathcart, J.V.; McKee, R.A. The kinetics of oxidation of Zircaloy-4 in steam at high temperatures. *J. Electrochem. Soc.* **1979**, *126*, 1105. [\[CrossRef\]](#)
58. Yan, Y.; Garrison, B.E.; Howell, M.; Bell, G.L. High-temperature oxidation kinetics of sponge-based E110 cladding alloy. *J. Nucl. Mater.* **2018**, *499*, 595–612. [\[CrossRef\]](#)
59. NRC. *50.46 Acceptance Criteria for Emergency Core Cooling Systems for Light-Water Nuclear Power Reactors*; US NRC: Washington, DC, USA, 2017.
60. Le Saux, M.; Brachet, J.-C.; Vandenberghe, V.; Ambard, A.; Chosson, R. Breakaway oxidation of zirconium alloys exposed to steam around 1000 °C. *Corros. Sci.* **2020**, *176*, 108936. [\[CrossRef\]](#)
61. Steinbrueck, M.; da Silva, F.O.; Grosse, M. Oxidation of Zircaloy-4 in steam-nitrogen mixtures at 600–1200 °C. *J. Nucl. Mater.* **2017**, *490*, 226–237. [\[CrossRef\]](#)
62. Steinbrück, M. Prototypical experiments relating to air oxidation of Zircaloy-4 at high temperatures. *J. Nucl. Mater.* **2009**, *392*, 531–544. [\[CrossRef\]](#)
63. Steinbrück, M.; Böttcher, M. Air oxidation of Zircaloy-4, M5[®] and ZIRLOTM cladding alloys at high temperatures. *J. Nucl. Mater.* **2011**, *414*, 276–285. [\[CrossRef\]](#)
64. Tang, C.; Stueber, M.; Seifert, H.J.; Steinbrueck, M. Protective coatings on zirconium-based alloys as accident-tolerant fuel (ATF) claddings. *Corros. Rev.* **2017**, *35*, 141–165. [\[CrossRef\]](#)

65. Bischoff, J.; Vauglin, C.; Delafoy, C.; Barberis, P.; Perche, D.; Guerin, B.; Vassault, J.; Brachet, J. Development of Cr-coated zirconium alloy cladding for enhanced accident tolerance. In Proceedings of the Top Fuel 2016, Boise, ID, USA, 11–16 September 2016; pp. 1165–1171.
66. Maier, B.; Yeom, H.; Johnson, G.; Dabney, T.; Walters, J.; Xu, P.; Romero, J.; Shah, H.; Sridharan, K. Development of cold spray chromium coatings for improved accident tolerant zirconium-alloy cladding. *J. Nucl. Mater.* **2019**, *519*, 247–254. [\[CrossRef\]](#)
67. Wei, T.; Zhang, R.; Yang, H.; Liu, H.; Qiu, S.; Wang, Y.; Du, P.; He, K.; Hu, X.; Dong, C. Microstructure, corrosion resistance and oxidation behavior of Cr-coatings on Zircaloy-4 prepared by vacuum arc plasma deposition. *Corros. Sci.* **2019**, *158*, 108077. [\[CrossRef\]](#)
68. Bryan, W.J.; Jones, D. Wear resistant coating for fuel cladding. Patent 5,268,946, 7 December 1993.
69. Gray, D.M.; White, D.W.; Andresen, P.L.; Kim, Y.J.; Lin, Y.P.; Curtis, T.C.; Patterson, C.B. Fuel Rod with Wear-Inhibiting Coating. U.S. Patent 11/780,537, 22 January 2009.
70. Kashkarov, E.B.; Nikitenkov, N.; Sutygina, A.; Obrosof, A.; Manakhov, A.; Polčák, J.; Weiß, S. Hydrogen absorption by Ti-implanted Zr-1Nb alloy. *Int. J. Hydrogen Energy* **2018**, *43*, 2484–2491. [\[CrossRef\]](#)
71. Kashkarov, E.; Nikitenkov, N.; Sutygina, A.; Laptev, R.; Bordulev, Y.; Obrosof, A.; Liedke, M.O.; Wagner, A.; Zak, A.; Weiß, S. Microstructure, defect structure and hydrogen trapping in zirconium alloy Zr-1Nb treated by plasma immersion Ti ion implantation and deposition. *J. Alloys Compd.* **2018**, *732*, 80–87. [\[CrossRef\]](#)
72. Kashkarov, E.; Sidelev, D.; Rombaeva, M.; Syrtanov, M.; Bleykher, G. Chromium coatings deposited by cooled and hot target magnetron sputtering for accident tolerant nuclear fuel claddings. *Surf. Coat. Technol.* **2020**, *389*, 125618. [\[CrossRef\]](#)
73. Lee, Y.; Lee, J.I.; No, H.C. Mechanical analysis of surface-coated zircaloy cladding. *Nucl. Eng. Technol.* **2017**, *49*, 1031–1043. [\[CrossRef\]](#)
74. Younker, I.; Fraton, M. Neutronic evaluation of coating and cladding materials for accident tolerant fuels. *Prog. Nucl. Energy* **2016**, *88*, 10–18. [\[CrossRef\]](#)
75. Kam, D.H.; Lee, J.H.; Lee, T.; Jeong, Y.H. Critical heat flux for SiC-and Cr-coated plates under atmospheric condition. *Ann. Nucl. Energy* **2015**, *76*, 335–342. [\[CrossRef\]](#)
76. Birks, N.; Meier, G.H.; Pettit, F.S. *Introduction to the High Temperature Oxidation of Metals*, 2nd ed.; Cambridge University Press: Cambridge, UK, 2006.
77. Young, D.J. *High Temperature Oxidation and Corrosion of Metals*, 2nd ed.; Elsevier: Amsterdam, The Netherlands, 2008.
78. Kofstad, P. *High Temperature Corrosion*; Elsevier Applied Science Publishers Ltd.: Amsterdam, The Netherlands, 1988.
79. Sarrazin, P.; Galerie, A.; Fouletier, J. *Mechanisms of High Temperature Corrosion*; Trans Tech Publications Ltd.: Bâch, Switzerland, 2008.
80. Pasamehmetoglu, K.; Massara, S.; Costa, D.; Bragg-Sitton, S.; Moatti, M.; Kurata, M.; Iracane, D.; Ivanova, T.; Bischoff, J.; Delafoy, C. *State-of-the-Art Report on Light Water Reactor Accident-Tolerant Fuels*; Organisation for Economic Co-Operation and Development: Paris, France, 2018.
81. Zhong, W.; Mouche, P.A.; Han, X.; Heuser, B.J.; Mandapaka, K.K.; Was, G.S. Performance of iron–chromium–aluminum alloy surface coatings on Zircaloy 2 under high-temperature steam and normal BWR operating conditions. *J. Nucl. Mater.* **2016**, *470*, 327–338. [\[CrossRef\]](#)
82. Kim, H.-G.; Kim, I.-H.; Jung, Y.-I.; Park, D.-J.; Park, J.-H.; Yang, J.-H.; Koo, Y.-H. Progress of surface modified Zr cladding development for ATF at KAERI. In Proceedings of the 2017 Water Reactor Fuel Performance Meeting, Ramada Plaza Jeju, Jeju Island, Korea, 10–14 September 2017; pp. 10–14.
83. Aydogan, E.; Weaver, J.S.; Maloy, S.A.; El-Atwani, O.; Wang, Y.Q.; Mara, N.A. Microstructure and mechanical properties of FeCrAl alloys under heavy ion irradiations. *J. Nucl. Mater.* **2018**, *503*, 250–262. [\[CrossRef\]](#)
84. Dabney, T.; Johnson, G.; Yeom, H.; Maier, B.; Walters, J.; Sridharan, K. Experimental evaluation of cold spray FeCrAl alloys coated zirconium-alloy for potential accident tolerant fuel cladding. *Nucl. Mater. Energy* **2019**, *21*, 100715. [\[CrossRef\]](#)
85. Gigax, J.G.; Kennas, M.; Kim, H.; Maier, B.R.; Yeom, H.; Johnson, G.O.; Sridharan, K.; Shao, L. Interface reactions and mechanical properties of FeCrAl-coated Zircaloy-4. *J. Nucl. Mater.* **2019**, *519*, 57–63. [\[CrossRef\]](#)
86. Park, D.J.; Kim, H.G.; Jung, Y.I.; Park, J.H.; Yang, J.H.; Koo, Y.H. Behavior of an improved Zr fuel cladding with oxidation resistant coating under loss-of-coolant accident conditions. *J. Nucl. Mater.* **2016**, *482*, 75–82. [\[CrossRef\]](#)
87. Brachet, J.-C.; Idarraga-Trujillo, I.; Le Flem, M.; Le Saux, M.; Vandenberghe, V.; Urvoy, S.; Rouesne, E.; Guilbert, T.; Toffolon-Masclat, C.; Tupin, M. Early studies on Cr-Coated Zircaloy-4 as enhanced accident tolerant nuclear fuel claddings for light water reactors. *J. Nucl. Mater.* **2019**, *517*, 268–285. [\[CrossRef\]](#)
88. Wang, X.; Guan, H.; Liao, Y.; Zhu, M.; Xu, C.; Jin, X.; Liao, B.; Xue, W.; Zhang, Y.; Bai, G.; et al. Enhancement of high temperature steam oxidation resistance of Zr-1Nb alloy with ZrO₂/Cr bilayer coating. *Corr. Sci.* **2021**, *187*, 109494. [\[CrossRef\]](#)
89. Yeom, H.; Sridharan, K. Cold spray technology in nuclear energy applications: A review of recent advances. *Ann. Nucl. Energy* **2021**, *150*, 107835. [\[CrossRef\]](#)
90. Kim, H.-G.; Kim, I.-H.; Jung, Y.-I.; Park, D.-J.; Park, J.-Y.; Koo, Y.-H. Adhesion property and high-temperature oxidation behavior of Cr-coated Zircaloy-4 cladding tube prepared by 3D laser coating. *J. Nucl. Mater.* **2015**, *465*, 531–539. [\[CrossRef\]](#)
91. Huang, M.; Li, Y.; Ran, G.; Yang, Z.; Wang, P. Cr-coated Zr-4 alloy prepared by electroplating and its in situ He⁺ irradiation behavior. *J. Nucl. Mater.* **2020**, *538*, 152240. [\[CrossRef\]](#)

92. Brachet, J.; Le Saux, M.; Le Flem, M.; Urvoy, S.; Rouesne, E.; Guilbert, T.; Cobac, C.; Lahogue, F.; Rousselot, J.; Tupin, M. On-going studies at CEA on chromium coated zirconium based nuclear fuel claddings for enhanced accident tolerant LWRs fuel. In Proceedings of the TopFuel, Zurich, Switzerland, 13–19 September 2015; pp. 13–19.
93. Wagih, M.; Spencer, B.; Hales, J.; Shirvan, K. Fuel performance of chromium-coated zirconium alloy and silicon carbide accident tolerant fuel claddings. *Ann. Nucl. Energy* **2018**, *120*, 304–318. [\[CrossRef\]](#)
94. Holzwarth, U.; Stamm, H. Mechanical and thermomechanical properties of commercially pure chromium and chromium alloys. *J. Nucl. Mater.* **2002**, *300*, 161–177. [\[CrossRef\]](#)
95. Ma, H.-B.; Yan, J.; Zhao, Y.-H.; Liu, T.; Ren, Q.-S.; Liao, Y.-H.; Zuo, J.-D.; Liu, G.; Yao, M.-Y. Oxidation behavior of Cr-coated zirconium alloy cladding in high-temperature steam above 1200 °C. *Npj Mater. Degrad.* **2021**, *5*, 1–11. [\[CrossRef\]](#)
96. Han, X.; Xue, J.; Peng, S.; Zhang, H. An interesting oxidation phenomenon of Cr coatings on Zry-4 substrates in high temperature steam environment. *Corros. Sci.* **2019**, *156*, 117–124. [\[CrossRef\]](#)
97. Le Saux, M.; Brachet, J.; Vandenberghe, V.; Gilbon, D.; Mardon, J.; Sebbari, B. Influence of pre-transient oxide on LOCA high temperature steam oxidation and post-quench mechanical properties of zircaloy-4 and M5™ cladding. In Proceedings of the Water Reactor Fuel Performance Meeting, paper T3-040, Chengdu, China, 11–14 September 2011.
98. Ribis, J.; Wu, A.; Brachet, J.-C.; Barcelo, F.; Arnal, B. Atomic-scale interface structure of a Cr-coated Zircaloy-4 material. *J. Mater. Sci.* **2018**, *53*, 9879–9895. [\[CrossRef\]](#)
99. Jiang, J.; Zhan, D.; Lv, J.; Ma, X.; He, X.; Wang, D.; Hu, Y.; Zhai, H.; Tu, J.; Zhang, W. Comparative study on the tensile cracking behavior of CrN and Cr coatings for accident-tolerant fuel claddings. *Surf. Coat. Technol.* **2021**, *409*, 126812. [\[CrossRef\]](#)
100. Wu, A.; Ribis, J.; Brachet, J.-C.; Clouet, E.; Lepître, F.; Bordas, E.; Arnal, B. HRTEM and chemical study of an ion-irradiated chromium/zircaloy-4 interface. *J. Nucl. Mater.* **2018**, *504*, 289–299. [\[CrossRef\]](#)
101. Kuprin, A.S.; Belous, V.A.; Voyevodin, V.N.; Vasilenko, R.L.; Ovcharenko, V.D.; Tolstolutsкая, G.D.; Kopanets, I.E.; Kolodiy, I.V. Irradiation resistance of vacuum arc chromium coatings for zirconium alloy fuel claddings. *J. Nucl. Mater.* **2018**, *510*, 163–167. [\[CrossRef\]](#)
102. Kuprin, A.S.; Vasilenko, R.L.; Tolstolutsкая, G.D.; Voyevodin, V.N.; Belous, V.A.; Ovcharenko, V.D.; Kopanets, I.E. Irradiation resistance of chromium coatings for ATF in the temperature range 300–550 °C. *J. Nucl. Mater.* **2021**, *549*, 152908. [\[CrossRef\]](#)
103. Chen, S.-L.; He, X.-J.; Yuan, C.-X. Recent studies on potential accident-tolerant fuel-cladding systems in light water reactors. *Nucl. Sci. Tech.* **2020**, *31*, 1–30. [\[CrossRef\]](#)
104. Kim, J.-M.; Ha, T.-H.; Kim, I.-H.; Kim, H.-G. Microstructure and oxidation behavior of CrAl laser-coated Zircaloy-4 alloy. *Metals* **2017**, *7*, 59. [\[CrossRef\]](#)
105. Park, D.J.; Jung, Y.I.; Park, J.H.; Lee, Y.H.; Choi, B.K.; Kim, H.G. Microstructural characterization of accident tolerant fuel cladding with Cr–Al alloy coating layer after oxidation at 1200° C in a steam environment. *Nucl. Eng. Technol.* **2020**, *52*, 2299–2305. [\[CrossRef\]](#)
106. Sidelev, D.V.; Kashkarov, E.B.; Syrtanov, M.S.; Krivobokov, V.P. Nickel-chromium (Ni-Cr) coatings deposited by magnetron sputtering for accident tolerant nuclear fuel claddings. *Surf. Coat. Technol.* **2019**, *369*, 69–78. [\[CrossRef\]](#)
107. Jin, D.; Yang, F.; Zou, Z.; Gu, L.; Zhao, X.; Guo, F.; Xiao, P. A study of the zirconium alloy protection by Cr₃C₂–NiCr coating for nuclear reactor application. *Surf. Coat. Technol.* **2016**, *287*, 55–60. [\[CrossRef\]](#)
108. Sridharan, K.; Harrington, S.; Johnson, A.; Licht, J.; Anderson, M.; Allen, T. Oxidation of plasma surface modified zirconium alloy in pressurized high temperature water. *Mater. Des.* **2007**, *28*, 1177–1185. [\[CrossRef\]](#)
109. Kim, H.-G.; Kim, I.-H.; Jung, Y.-I.; Park, D.-J.; Park, J.-Y.; Koo, Y.-H. Microstructure and mechanical strength of surface ODS treated Zircaloy-4 sheet using laser beam scanning. *Nucl. Eng. Technol.* **2014**, *46*, 521–528. [\[CrossRef\]](#)
110. Kim, H.-G.; Yang, J.-H.; Kim, W.-J.; Koo, Y.-H. Development status of accident-tolerant fuel for light water reactors in Korea. *Nucl. Eng. Technol.* **2016**, *48*, 1–15. [\[CrossRef\]](#)
111. Yeh, J.W.; Chen, S.K.; Lin, S.J.; Gan, J.Y.; Chin, T.S.; Shun, T.T.; Tsau, C.H.; Chang, S.Y. Nanostructured high-entropy alloys with multiple principal elements: Novel alloy design concepts and outcomes. *Adv. Eng. Mater.* **2004**, *6*, 299–303. [\[CrossRef\]](#)
112. Fereiduni, E.; Ghasemi, A.; Elbestawi, M. Characterization of composite powder feedstock from powder bed fusion additive manufacturing perspective. *Materials* **2019**, *12*, 3673. [\[CrossRef\]](#)
113. Do, H.-S.; Lee, B.-J. Origin of radiation resistance in multi-principal element alloys. *Sci. Rep.* **2018**, *8*, 1–9.
114. Gao, L.; Liao, W.; Zhang, H.; Surjadi, J.U.; Sun, D.; Lu, Y. Microstructure, mechanical and corrosion behaviors of CoCrFeNiAl_{0.3} high entropy alloy (HEA) films. *Coatings* **2017**, *7*, 156. [\[CrossRef\]](#)
115. Zhang, W.; Tang, R.; Yang, Z.; Liu, C.; Chang, H.; Yang, J.; Liao, J.; Yang, Y.; Liu, N. Preparation, structure, and properties of an AlCrMoNbZr high-entropy alloy coating for accident-tolerant fuel cladding. *Surf. Coat. Technol.* **2018**, *347*, 13–19. [\[CrossRef\]](#)
116. Zhang, W.; Wang, M.; Wang, L.; Liu, C.; Chang, H.; Yang, J.; Liao, J.; Yang, Y.; Liu, N. Interface stability, mechanical and corrosion properties of AlCrMoNbZr/(AlCrMoNbZr) N high-entropy alloy multilayer coatings under helium ion irradiation. *Appl. Surf. Sci.* **2019**, *485*, 108–118. [\[CrossRef\]](#)
117. Zhang, W.; Tang, R.; Yang, Z.; Liu, C.; Chang, H.; Yang, J.; Liao, J.; Yang, Y.; Liu, N. Preparation, structure, and properties of high-entropy alloy multilayer coatings for nuclear fuel cladding: A case study of AlCrMoNbZr/(AlCrMoNbZr) N. *J. Nucl. Mater.* **2018**, *512*, 15–24. [\[CrossRef\]](#)
118. Tao, Z.; Wang, P.; Wang, C.; Ma, Z.; Zhang, Y.; Xue, F.; Bai, G.; Yuan, Y.; Lan, R. Design and characterisation of AlCrFeCuNb_x alloys for accident-tolerant fuel cladding. *J. Alloys Compd.* **2021**, *859*, 157805. [\[CrossRef\]](#)

119. Zhang, Z.; Han, E.-H.; Xiang, C. Irradiation behaviors of two novel single-phase bcc-structure high-entropy alloys for accident-tolerant fuel cladding. *J. Mater. Sci. Technol.* **2021**, *84*, 230–238. [\[CrossRef\]](#)
120. Pickering, E.J.; Carruthers, A.W.; Barron, P.J.; Middleburgh, S.C.; Armstrong, D.E.; Gandy, A.S. High-Entropy Alloys for Advanced Nuclear Applications. *Entropy* **2021**, *23*, 98. [\[CrossRef\]](#)
121. Yun, D.; Lu, C.; Zhou, Z.; Wu, Y.; Liu, W.; Guo, S.; Shi, T.; Stubbins, J.F. Current state and prospect on the development of advanced nuclear fuel system materials: A review. *Mater. Rep. Energy* **2021**. [\[CrossRef\]](#)
122. Khatkhatay, F.; Jiao, L.; Jian, J.; Zhang, W.; Jiao, Z.; Gan, J.; Zhang, H.; Zhang, X.; Wang, H. Superior corrosion resistance properties of TiN-based coatings on Zircaloy tubes in supercritical water. *J. Nucl. Mater.* **2014**, *451*, 346–351. [\[CrossRef\]](#)
123. Kashkarov, E.; Nikitenkov, N.; Sutygina, A.; Bezmaternykh, A.; Kudiiarov, V.; Syrtanov, M.; Pryamushko, T. Hydrogenation behavior of Ti-implanted Zr-1Nb alloy with TiN films deposited using filtered vacuum arc and magnetron sputtering. *Appl. Surf. Sci.* **2018**, *432*, 207–213. [\[CrossRef\]](#)
124. Tunes, M.A.; Da Silva, F.C.; Camara, O.; Schön, C.G.; Sagás, J.C.; Fontana, L.C.; Donnelly, S.E.; Greaves, G.; Edmondson, P.D. Energetic particle irradiation study of TiN coatings: Are these films appropriate for accident tolerant fuels? *J. Nucl. Mater.* **2018**, *512*, 239–245. [\[CrossRef\]](#)
125. Khatkhatay, F.; Jian, J.; Jiao, L.; Su, Q.; Gan, J.; Cole, J.I.; Wang, H. Diffusion barrier properties of nitride-based coatings on fuel cladding. *J. Alloys Compd.* **2013**, *580*, 442–448. [\[CrossRef\]](#)
126. Xiao, W.; Chen, H.; Liu, X.; Tang, D.; Deng, H.; Zou, S.; Ren, Y.; Zhou, X.; Lei, M. Thermal shock resistance of TiN-, Cr-, and TiN/Cr-coated zirconium alloy. *J. Nucl. Mater.* **2019**, *526*, 151777. [\[CrossRef\]](#)
127. Alat, E.; Motta, A.T.; Comstock, R.J.; Partezana, J.M.; Wolfe, D.E. Ceramic coating for corrosion (c3) resistance of nuclear fuel cladding. *Surf. Coat. Technol.* **2015**, *281*, 133–143. [\[CrossRef\]](#)
128. Alat, E.; Motta, A.T.; Comstock, R.J.; Partezana, J.M.; Wolfe, D.E. Multilayer (TiN, TiAlN) ceramic coatings for nuclear fuel cladding. *J. Nucl. Mater.* **2016**, *478*, 236–244. [\[CrossRef\]](#)
129. Alat, E.; Brova, M.; Younker, I.; Motta, A.; Fratoni, M.; Wolfe, D. Neutronic and mechanical evaluation of rare earth doped and undoped nitride-based coatings for accident tolerant fuels. *J. Nucl. Mater.* **2019**, *518*, 419–430. [\[CrossRef\]](#)
130. Daub, K.; Van Nieuwenhove, R.; Nordin, H. Investigation of the impact of coatings on corrosion and hydrogen uptake of Zircaloy-4. *J. Nucl. Mater.* **2015**, *467*, 260–270. [\[CrossRef\]](#)
131. Van Nieuwenhove, R.; Andersson, V.; Balak, J.; Oberländer, B. In-Pile testing of CrN, TiAlN, and AlCrN coatings on zircaloy cladding in the Halden reactor. *ASTM Int.* **2018**, 965–982. [\[CrossRef\]](#)
132. Meng, C.; Yang, L.; Wu, Y.; Tan, J.; Dang, W.; He, X.; Ma, X. Study of the oxidation behavior of CrN coating on Zr alloy in air. *J. Nucl. Mater.* **2019**, *515*, 354–369. [\[CrossRef\]](#)
133. Krejčí, J.; Ševeček, M.; Cvrček, L.; Kabátová, J.; Manoch, F. Chromium and chromium nitride coated cladding for nuclear reactor fuel. In Proceedings of the 20th International Corrosion Congress, EUROCORR, Prague, Czech Republic, 3–7 September 2017.
134. Krejčí, J.; Ševeček, M.; Kabátová, J.; Manoch, F.; Kočí, J.; Cvrček, L.; Málek, J.; Krum, S.; Šutta, P.; Bublíková, P. Experimental behavior of chromium-based coatings. In Proceedings of the TopFuel, Prague, Czech Republic, 30 September–4 October 2018; pp. 1–13.
135. Song, J.; Huang, Z.; Qin, Y.; Wang, H.; Shi, M. Effects of Zirconium Silicide on the Vulcanization, Mechanical and Ablation Resistance Properties of Ceramifiable Silicone Rubber Composites. *Polymers* **2020**, *12*, 496. [\[CrossRef\]](#) [\[PubMed\]](#)
136. Yeom, H.; Maier, B.; Mariani, R.; Bai, D.; Fronek, S.; Xu, P.; Sridharan, K. Magnetron sputter deposition of zirconium-silicide coating for mitigating high temperature oxidation of zirconium-alloy. *Surf. Coat. Technol.* **2017**, *316*, 30–38. [\[CrossRef\]](#)
137. Yeom, H.; Lockhart, C.; Mariani, R.; Xu, P.; Corradini, M.; Sridharan, K. Evaluation of steam corrosion and water quenching behavior of zirconium-silicide coated LWR fuel claddings. *J. Nucl. Mater.* **2018**, *499*, 256–267. [\[CrossRef\]](#)
138. Terrani, K.A.; Pint, B.A.; Parish, C.M.; Silva, C.M.; Snead, L.L.; Katoh, Y. Silicon carbide oxidation in steam up to 2 MPa. *J. Am. Ceram. Soc.* **2014**, *97*, 2331–2352. [\[CrossRef\]](#)
139. Lee, K.; Kim, D.; Yoon, Y.S. SiC/Si thin film deposited on zircaloy to improved accident tolerant fuel cladding. *Thin Solid Film.* **2018**, *660*, 221–230. [\[CrossRef\]](#)
140. Kashkarov, E.B.; Syrtanov, M.S.; Murashkina, T.L.; Kurochkin, A.V.; Shanenkova, Y.; Obrosova, A. Hydrogen sorption kinetics of SiC-coated Zr-1Nb alloy. *Coatings* **2019**, *9*, 31. [\[CrossRef\]](#)
141. Usui, T.; Sawada, A.; Amaya, M.; Suzuki, A.; Chikada, T.; Terai, T. SiC coating as hydrogen permeation reduction and oxidation resistance for nuclear fuel cladding. *J. Nucl. Sci. Technol.* **2015**, *52*, 1318–1322. [\[CrossRef\]](#)
142. Bao, W.; Xue, J.; Liu, J.-X.; Wang, X.; Gu, Y.; Xu, F.; Zhang, G.-J. Coating SiC on Zircaloy-4 by magnetron sputtering at room temperature. *J. Alloys Compd.* **2018**, *730*, 81–87. [\[CrossRef\]](#)
143. Al-Olayyan, Y.; Fuchs, G.; Baney, R.; Tulenko, J. The effect of Zircaloy-4 substrate surface condition on the adhesion strength and corrosion of SiC coatings. *J. Nucl. Mater.* **2005**, *346*, 109–119. [\[CrossRef\]](#)
144. Baney, R.H.; Butt, D.; Demkowicz, P.; Tulenko, J.S. *An Innovative Ceramic Corrosion Protection System for Zircaloy Cladding*; University of Florida (US): Gainesville, FL, USA, 2003.
145. Tang, C.; Steinbrueck, M.; Grosse, M.; Ulrich, S.; Stueber, M.; Seifert, H.J. Evaluation of magnetron sputtered protective Zr-C-Al coatings for accident tolerant Zircaloy claddings. In Proceedings of the Water Reactor Fuel Performance Meeting, Jeju Island, Korea, 10–14 September 2017.

146. Michau, A.; Maury, F.; Schuster, F.; Lomello, F.; Brachet, J.-C.; Rouesne, E.; Le Saux, M.; Boichot, R.; Pons, M. High-temperature oxidation resistance of chromium-based coatings deposited by DLI-MOCVD for enhanced protection of the inner surface of long tubes. *Surf. Coat. Technol.* **2018**, *349*, 1048–1057. [\[CrossRef\]](#)
147. Michau, A.; Maury, F.; Schuster, F.; Nuta, I.; Gazal, Y.; Boichot, R.; Pons, M. Chromium carbide growth by direct liquid injection chemical vapor deposition in long and narrow tubes, experiments, modeling and simulation. *Coatings* **2018**, *8*, 220. [\[CrossRef\]](#)
148. Michau, A.; Gazal, Y.; Addou, F.; Maury, F.; Duguet, T.; Boichot, R.; Pons, M.; Monsifrot, E.; Maskrot, H.; Schuster, F. Scale up of a DLI-MOCVD process for the internal treatment of a batch of 16 nuclear fuel cladding segments with a CrCx protective coating. *Surf. Coat. Technol.* **2019**, *375*, 894–902. [\[CrossRef\]](#)
149. Yang, Z.; Niu, Y.; Xue, J.; Liu, T.; Chang, C.; Zheng, X. Steam oxidation resistance of plasma sprayed chromium-containing coatings at 1200 °C. *Mater. Corros.* **2019**, *70*, 37–47. [\[CrossRef\]](#)
150. Lyu, J.; Kashkarov, E.; Travitzky, N.; Syrtanov, M.; Lider, A. Sintering of MAX-phase materials by spark plasma and other methods. *J. Mater. Sci.* **2020**, *56*, 1–36.
151. Barsoum, M.W. The MN+ 1AXN phases: A new class of solids: Thermodynamically stable nanolaminates. *Prog. Solid State Chem.* **2000**, *28*, 201–281. [\[CrossRef\]](#)
152. Barsoum, M.W.; El-Raghy, T. The MAX phases: Unique new carbide and nitride materials: Ternary ceramics turn out to be surprisingly soft and machinable, yet also heat-tolerant, strong and lightweight. *Am. Sci.* **2001**, *89*, 334–343. [\[CrossRef\]](#)
153. Garcia-Diaz, B.; Olson, L.; Verst, C.; Sindelar, R.; Hoffman, E.; Hauch, B.; Maier, B.; Sridharan, K. MAX phase coatings for accident tolerant nuclear fuel. *Trans. Am. Nucl. Soc* **2014**, *110*, 994–996.
154. Tallman, D.J.; Anasori, B.; Barsoum, M.W. A critical review of the oxidation of Ti₂AlC, Ti₃AlC₂ and Cr₂AlC in air. *Mater. Res. Lett.* **2013**, *1*, 115–125. [\[CrossRef\]](#)
155. Li, W.; Wang, Z.; Shuai, J.; Xu, B.; Wang, A.; Ke, P. A high oxidation resistance Ti₂AlC coating on Zirlo substrates for loss-of-coolant accident conditions. *Ceram. Int.* **2019**, *45*, 13912–13922. [\[CrossRef\]](#)
156. Maier, B.R.; Garcia-Diaz, B.L.; Hauch, B.; Olson, L.C.; Sindelar, R.L.; Sridharan, K. Cold spray deposition of Ti₂AlC coatings for improved nuclear fuel cladding. *J. Nucl. Mater.* **2015**, *466*, 712–717. [\[CrossRef\]](#)
157. Tang, C.; Steinbrueck, M.; Stueber, M.; Grosse, M.; Yu, X.; Ulrich, S.; Seifert, H.J. Deposition, characterization and high-temperature steam oxidation behavior of single-phase Ti₂AlC-coated Zircaloy-4. *Corros. Sci.* **2018**, *135*, 87–98. [\[CrossRef\]](#)
158. Roberts, D.A. Magnetron Sputtering and Corrosion of Ti-Al-C and Cr-Al-C Coatings for Zr-Alloy Nuclear Fuel Cladding. Master's Thesis, University of Tennessee, Knoxville, TN, USA, 2016.
159. Tang, C.; Steinbrueck, M.; Grosse, M.; Ulrich, S.; Stueber, M.; Seifert, H.J. Improvement of the high-temperature oxidation resistance of Zr alloy cladding by surface modification with aluminum-containing ternary carbide coatings. In Proceedings of the 2018 International Congress on Advances in Nuclear Power Plants, Charlotte, NC, USA, 8–11 April 2018.
160. Imtyazuddin, M.; Mir, A.H.; Tunes, M.A.; Vishnyakov, V.M. Radiation resistance and mechanical properties of magnetron-sputtered Cr₂AlC thin films. *J. Nucl. Mater.* **2019**, *526*, 151742. [\[CrossRef\]](#)
161. Tang, C.; Grosse Karl, M.; Trtik, P.; Steinbrück, M.; Stüber, M.; Seifert, H.J. H₂ Permeation Behavior of Cr₂AlC and Ti₂AlC MAX Phase Coated Zircaloy4 by Neutron Radiography. *Acta Polytech.* **2018**, *58*, 69–76. [\[CrossRef\]](#)
162. Wang, Z.; Ma, G.; Liu, L.; Wang, L.; Ke, P.; Xue, Q.; Wang, A. High-performance Cr₂AlC MAX phase coatings: Oxidation mechanisms in the 900–1100 C temperature range. *Corros. Sci.* **2020**, *167*, 108492. [\[CrossRef\]](#)
163. Opila, E.J.; Jacobson, N.S.; Myers, D.L.; Copland, E.H. Predicting oxide stability in high-temperature water vapor. *JOM* **2006**, *58*, 22–28. [\[CrossRef\]](#)
164. Doyle, P.J.; Raiman, S.S.; Rebak, R.; Terrani, K.A. Characterization of the hydrothermal corrosion behavior of ceramics for accident tolerant fuel cladding. In Proceedings of the 18th International Conference on Environmental Degradation of Materials in Nuclear Power Systems—Water Reactors, Portland, OR, USA, 13–17 August 2017.
165. Kashkarov, E.; Sidelev, D.; Syrtanov, M.; Tang, C.; Steinbrück, M. Oxidation kinetics of Cr-coated zirconium alloy: Effect of coating thickness and microstructure. *Corros. Sci.* **2020**, *175*, 108883. [\[CrossRef\]](#)
166. Brachet, J.-C.; Rouesne, E.; Ribis, J.; Guilbert, T.; Urvoy, S.; Nony, G.; Toffolon-Masclet, C.; Le Saux, M.; Chaabane, N.; Palancher, H. High temperature steam oxidation of chromium-coated zirconium-based alloys: Kinetics and process. *Corros. Sci.* **2020**, *167*, 108537. [\[CrossRef\]](#)
167. Novák, O.; Ševeček, M. Neutronic analysis of the candidate multi-layer cladding materials with enhanced accident tolerance for wwr reactors. *Acta Polytech. Ctú Proc.* **2018**, *14*, 27–33. [\[CrossRef\]](#)
168. Yang, J.; Stegmaier, U.; Tang, C.; Steinbrück, M.; Große, M.; Wang, S.; Seifert, H.J. High temperature Cr-Zr interaction of two types of Cr-coated Zr alloys in inert gas environment. *J. Nucl. Mater.* **2021**, *547*, 152806. [\[CrossRef\]](#)
169. Li, G.; Liu, Y.; Zhang, Y.; Li, H.; Wang, X.; Zheng, M.; Li, Y. High Temperature Anti-Oxidation Behavior and Mechanical Property of Radio Frequency Magnetron Sputtered Cr Coating. *Metals* **2020**, *10*, 1509. [\[CrossRef\]](#)
170. Umretiya, R.V.; Elward, B.; Lee, D.; Anderson, M.; Rebak, R.B.; Rojas, J.V. Mechanical and chemical properties of PVD and cold spray Cr-coatings on Zircaloy-4. *J. Nucl. Mater.* **2020**, *541*, 152420. [\[CrossRef\]](#)
171. Thornton, J.A. Influence of apparatus geometry and deposition conditions on the structure and topography of thick sputtered coatings. *J. Vac. Sci. Technol.* **1974**, *11*, 666–670. [\[CrossRef\]](#)
172. Anders, A. A structure zone diagram including plasma-based deposition and ion etching. *Thin Solid Film.* **2010**, *518*, 4087–4090. [\[CrossRef\]](#)

173. Efeoglu, I.; Arnell, R.; Tinston, S.; Teer, D. The mechanical and tribological properties of titanium aluminium nitride coatings formed in a four magnetron closed-field sputtering system. *Surf. Coat. Technol.* **1993**, *57*, 117–121. [\[CrossRef\]](#)
174. Sarakinos, K.; Alami, J.; Konstantinidis, S. High power pulsed magnetron sputtering: A review on scientific and engineering state of the art. *Surf. Coat. Technol.* **2010**, *204*, 1661–1684. [\[CrossRef\]](#)
175. Ougier, M.; Michau, A.; Lomello, F.; Schuster, F.; Maskrot, H.; Schlegel, M.L. High-temperature oxidation behavior of HiPIMS as-deposited Cr–Al–C and annealed Cr₂AlC coatings on Zr-based alloy. *J. Nucl. Mater.* **2020**, *528*, 151855. [\[CrossRef\]](#)
176. Liu, J.; Cui, Z.; Ma, D.; Lu, J.; Cui, Y.; Li, C.; Liu, W.; Hao, Z.; Hu, P.; Yao, M. Investigation of oxidation behaviors of coated Zircaloy as accident-tolerant fuel with CrAlN and CrAlSiN coatings in high-temperature steam. *Corros. Sci.* **2020**, *175*, 108896. [\[CrossRef\]](#)
177. Han, X.; Wang, Y.; Peng, S.; Zhang, H. Oxidation behavior of FeCrAl coated Zry-4 under high temperature steam environment. *Corros. Sci.* **2019**, *149*, 45–53. [\[CrossRef\]](#)
178. Park, J.-H.; Kim, H.-G.; Park, J.-y.; Jung, Y.-I.; Park, D.-J.; Koo, Y.-H. High temperature steam-oxidation behavior of arc ion plated Cr coatings for accident tolerant fuel claddings. *Surf. Coat. Technol.* **2015**, *280*, 256–259. [\[CrossRef\]](#)
179. Yeom, H.; Maier, B.; Johnson, G.; Dabney, T.; Lenling, M.; Sridharan, K. High temperature oxidation and microstructural evolution of cold spray chromium coatings on Zircaloy-4 in steam environments. *J. Nucl. Mater.* **2019**, *526*, 151737. [\[CrossRef\]](#)
180. Wang, Y.; Zhou, W.; Wen, Q.; Ruan, X.; Luo, F.; Bai, G.; Qing, Y.; Zhu, D.; Huang, Z.; Zhang, Y. Behavior of plasma sprayed Cr coatings and FeCrAl coatings on Zr fuel cladding under loss-of-coolant accident conditions. *Surf. Coat. Technol.* **2018**, *344*, 141–148. [\[CrossRef\]](#)
181. Bhanumurthy, K.; Kale, G.; Khera, S. Reaction diffusion in the zirconium-iron system. *J. Nucl. Mater.* **1991**, *185*, 208–213. [\[CrossRef\]](#)
182. Wang, X.; Wei, K.; Guan, H.; Xu, C.; Xue, W.; Zhang, Y.; Wang, R. High temperature oxidation of Zr1Nb alloy with plasma electrolytic oxidation coating in 900–1200° C steam environment. *Surf. Coat. Technol.* **2021**, *407*, 126768. [\[CrossRef\]](#)
183. Krejčí, J.; Kabátová, J.; Manoch, F.; Kočí, J.; Cvrček, L.; Málek, J.; Krum, S.; Šutta, P.; Bublíková, P.; Halodová, P. Development and testing of multicomponent fuel cladding with enhanced accidental performance. *Nucl. Eng. Technol.* **2020**, *52*, 597–609. [\[CrossRef\]](#)
184. Azevedo, C. Selection of fuel cladding material for nuclear fission reactors. *Eng. Fail. Anal.* **2011**, *18*, 1943–1962. [\[CrossRef\]](#)
185. Fejt, F.; Sevecek, M.; Frybort, J.; Novak, O. Study on neutronics of VVER-1200 with accident tolerant fuel cladding. *Ann. Nucl. Energy* **2019**, *124*, 579–591. [\[CrossRef\]](#)
186. Tiwari, G.; Sharma, B.; Raghunathan, V.; Patil, R. Self-and solute-diffusion in dilute zirconium-niobium alloys in β -phase. *J. Nucl. Mater.* **1973**, *46*, 35–40. [\[CrossRef\]](#)
187. Patil, R.; Kale, G.; Garg, S. Chemical diffusion in Zr Nb system. *J. Nucl. Mater.* **1995**, *223*, 169–173. [\[CrossRef\]](#)
188. Graedel, T.E.; Harper, E.; Nassar, N.T.; Nuss, P.; Reck, B.K. Criticality of metals and metalloids. *Proc. Natl. Acad. Sci. USA* **2015**, *112*, 4257–4262. [\[CrossRef\]](#)
189. Chen, P.; Qiu, B.; Li, Y.; Wu, Y.; Hui, Y.; Deng, Y.; Zhang, K. An evaluation on in-pile behaviors of SiCf/SiC cladding under normal and accident conditions with updated FROBA-ATF code. *Nucl. Eng. Technol.* **2020**, *53*, 1236–1249. [\[CrossRef\]](#)
190. Doyle, P.J.; Koyanagi, T.; Ang, C.; Snead, L.; Mouche, P.; Katoh, Y.; Raiman, S.S. Evaluation of the effects of neutron irradiation on first-generation corrosion mitigation coatings on SiC for accident-tolerant fuel cladding. *J. Nucl. Mater.* **2020**, *536*, 152203. [\[CrossRef\]](#)
191. Cinbiz, M.N.; Brown, N.; Lowden, R.R.; Gussev, M.N.; Linton, K.D.; Terrani, K.A. *Report on Design and Failure Limits of SiC/SiC and FeCrAl ATF Cladding Concepts under RIA*; Oak Ridge National Lab. (ORNL): Oak Ridge, TN, USA, 2018.
192. Musil, J.; Sklenka, J.; Prochazka, J. Protective over-layer coating preventing cracking of thin films deposited on flexible substrates. *Surf. Coat. Technol.* **2014**, *240*, 275–280. [\[CrossRef\]](#)
193. Musil, J.; Sklenka, J.; Čerstvý, R. Protection of brittle film against cracking. *Appl. Surf. Sci.* **2016**, *370*, 306–311. [\[CrossRef\]](#)
194. Musil, J. Flexible hard nanocomposite coatings. *Rsc. Adv.* **2015**, *5*, 60482–60495. [\[CrossRef\]](#)
195. Sidelev, D.V.; Syrtanov, M.S.; Ruchkin, S.E.; Pirozhkov, A.V.; Kashkarov, E.B. Protection of Zr Alloy under High-Temperature Air Oxidation: A Multilayer Coating Approach. *Coatings* **2021**, *11*, 227. [\[CrossRef\]](#)